The effect of realistic nuclear charge distributions on atomic levels and transitions

Asimina Papoulia

Master Thesis

Supervisors: Gillis Carlsson & Jörgen Ekman

Division of Mathematical Physics, Lund University

Spring 2015

LUND UNIVERSITY

Mathematical Physics
Lund University

The effect of realistic nuclear charge distributions on atomic levels and transitions

Asimina Papoulia

Master Thesis

Supervisors: Gillis Carlsson & Jörgen Ekman

Division of Mathematical Physics, Lund University

Abstract

Analogue atomic spectral lines from different isotopes display a small shift in energy, commonly referred as the frequency isotope shift. One of the components of the isotope shift is the field shift, which depends on the extent and the shape of the nuclear charge density distribution. In this work, we investigate how sensitive field shifts are with respect to variations in the nuclear size and shapes. It is found that realistic shapes of nuclei can have a considerable effect in the prediction of the field shifts. Using a novel approach, we demonstrate the possibility to extract new information concerning the nuclear charge densities from the observed field shifts.

Contents

1 Introduction

The abundance of an isotope for a particular element varies between different astronomical objects and on a long-term scale it also varies from time to time depending on its decay rate. Therefore, the knowledge of the origin and evolution process of the astronomical objects existing in the Milky Way and other Galaxies depends not only on their elemental but also on their isotopic composition. Although the chemical composition of the Earth is well known, the study of the isotopes abundance in various stars and other planets is still of great interest. In addition, such studies are not restricted to the natural elements. They can also be expanded into the investigation of radioactive isotope abundances, artificially produced in laboratories.

Light coming from astronomical objects can be analyzed through the resulting spectra. Most commonly the energy spectra consist of several lines of different wave-lengths and intensities. For a particular element, the spectra of the various isotopes are very similar. A small shift in wave-length is however observed, known as the frequency isotope shift. As a result, the intensity of such peaks represents the isotopes abundance. By measuring the difference in frequency between two peaks representing analogue transitions, we can calculate the corresponding difference between the nuclear radii of the isotopes represented by these peaks. Thus, by using one isotope as reference we can identify the existing variety of isotopes.

For light nuclei, the difference in frequency is dominated by the difference in the second order radial moment $\delta \langle r^2 \rangle$, since the contribution of higher order radial moments of the nuclear charge density distribution on the frequency shift is almost negligible. However, in heavier systems the higher moments contribute to a particular percentage to this shift. Therefore, further conclusions can be drawn on the deformation, density wiggles etc. of the nuclear charge distributions in such systems. The main objective of this thesis is to study the effect of the higher order radial moments from realistic charge distributions on the frequency isotope shift in these heavy nuclear systems. We restrict ourselves to highly ionized lithium-like atomic systems, since for such systems the calculations become simplified.

Chapter 2 provides the theoretical background needed in order to calculate the nuclear densities, as well as the atomic levels and transition energies. Next, chapter 3 illustrates the validity of the nuclear interaction by performing a systematic study of the higher order radial moments of the nuclear charge density distributions. A reformulation of the field shift component of the isotope shift is introduced, in chapter 4, for the heavy nuclear systems. The reformulated field shift is, in chapter 5, used in order to estimate the effect that the realistic nuclear distributions have on the atomic levels and transitions. At last, it is explained how the observed isotope shifts can be used in order to extract the nuclear radial moments and therefore draw conclusions on the nuclear size and shape of the isotopes.

2 Theory

2.1 Hartree-Fock method

In microscopic systems the treatment of many-body problems is not a trivial task, even if the number of particles is not large. It is well known that in the simplest one-particle case of a Hydrogen atom, the Schrödinger equation can have an exact solution from which the eigenfunctions and eigenvalues of the system are obtained. However, for a N particle

system the Schrödinger equation is impossible to solve exactly. Therefore, methods have been developed to make it possible to obtain an approximate solution for such systems, by reducing the case to a one-particle problem. These approximations are called mean-field methods. In particular, Hartree-Fock (HF) is a mean-field method widely used for the description of many-body systems, constituting a principal tool for the description of both nuclear and atomic states. Furthermore, the HF method constitutes the starting point for the formulation of more sophisticated methods, like BCS and Hartree-Fock-Bogoliubov (HFB), which will be discussed in the upcoming section 2.2.

2.1.1 Hartree-Fock approximation

The main idea of the Hartree-Fock method is based on the assumption that the potential between the numerous particles of a system can be approximated by an averaged single-particle (mean-field) potential, so that the Hamiltonian of this many-body system is reduced to a single-particle Hamiltonian. This procedure is known as the Hartree approximation. Initially the Hamiltonian has the following form:

$$\hat{H} = \hat{T} + \hat{V} = -\frac{1}{2m}\sum_{i=1}^{n}\nabla_i^2 + \frac{1}{2}\sum_{i\neq j}^{n} u(\vec{r_i}, \vec{r_j}),$$

where the first term is the sum of the kinetic energy of all individual particles and the second term represents the potential energy between two particles, summed up for all possible combinations. The factor of $\frac{1}{2}$ ensures that terms like $u(\vec{r_1}, \vec{r_2})$ and $u(\vec{r_2}, \vec{r_1})$ are taken into account only once. The $i \neq j$ restriction on the sum ensures that particles do not interact with themselves. After the approximation the Hamiltonian above reduces to a one-particle Hamiltonian:

$$\hat{H}_{Hartree} = -\frac{1}{2m}\nabla^2 + V_H(\vec{r}).$$

However, this method does not take into account the fermionic nature of particles. To achieve this, the Hartree-Fock approximation makes the assumption that the total wave functions of the interacting particles could take the form of a Slater determinant, so that they obey the antisymmetry property. The linear eigenvalue problem then has the form:

$$\hat{H}_{HF}\left|\psi\right\rangle = E^{HF}\left|\psi\right\rangle,$$

with an additional Fock term V_F included now in the potential of the total Hartree-Fock Hamiltonian. For n-particles occupying n different orbitals $\{\phi_i\}_{i=1...n}$ the wave function ψ is a linear combination of products of these orbitals ϕ_i, with their coordinates $\{\overrightarrow{r_i}\}_{i=1...n}$ permuted in all possible ways with a change of sign when the number of two-coordinate permutations (p) is odd [3]:

$$\psi(\overrightarrow{r_1}, \overrightarrow{r_2}, ..., \overrightarrow{r_n}) = \sum_{P}\frac{(-1)^p}{\sqrt{n!}}P[\phi_1(\overrightarrow{r_1})\phi_2(\overrightarrow{r_2})...\phi_n(\overrightarrow{r_n})].$$

The sum over P means the sum over all possible permutations of the particles coordinates and p is the number of two-coordinate permutations required to obtain the product of orbitals in its initial form, i.e. $\phi_1(\overrightarrow{r_1})\phi_2(\overrightarrow{r_2})...\phi_n(\overrightarrow{r_n})$. Therefore, the ansatz we make has the form

of a Slater determinant, which (normalized for a combination of n particles) can also be equivalently written:

$$\psi(\overrightarrow{r_1},\overrightarrow{r_2},...,\overrightarrow{r_n}) = \frac{1}{\sqrt{n!}}\begin{vmatrix} \phi_1(\overrightarrow{r_1}) & \phi_2(\overrightarrow{r_1}) & \dots & \phi_n(\overrightarrow{r_1}) \\ \phi_1(\overrightarrow{r_2}) & \phi_2(\overrightarrow{r_2}) & \dots & \phi_n(\overrightarrow{r_2}) \\ \vdots & \vdots & \ddots & \vdots \\ \phi_1(\overrightarrow{r_n}) & \phi_2(\overrightarrow{r_n}) & \dots & \phi_n(\overrightarrow{r_n}) \end{vmatrix}.$$

For a given complete set of orthonormal orbitals $\{\phi_i\}_{i=1...n}$ we can construct a complete set of all possible Slater determinants, which are also orthonormal. This complete set of orthonormal Slater determinants is said to form the Fock space [3].

2.1.2 Variational principle

To obtain the most appropriate wave function, we must choose among all possible Slater determinants ψ the one that yields the lowest total energy. According to the variational principle:

$$E_{g.s.}^{HF} \leq \frac{\left\langle \psi \mid \hat{H} \mid \psi \right\rangle}{\langle \psi \mid \psi \rangle},$$

the ground state (g.s.) energy will always be the lowest bound of a variational calculation. For a trial wave function then the ground state energy is always larger than or ideally equal to the exact ground state energy:

$$E_{g.s.}^{HF} = \left\langle \psi \left| \hat{H}_{HF} \right| \psi \right\rangle \geq E_{g.s.}^{true}$$

Therefore, the closer the trial wave function is to the exact ground state wave function the more representative it will be for the given system of interacting particles. The expectation value of the Hartree-Fock Hamiltonian will be calculated by using the occupation number representation [23]. We will then minimize the total ground state energy with respect to all possible choices of the n existing orbitals $\{\phi_i\}_{i=1...n}$ by applying the method of Lagrange multipliers.

Thus, we vary the total energy with respect to an infinitesimal change in the orbitals $\phi_i(\overrightarrow{r})$, e.g. $\delta E = \lim_{\varepsilon\to 0}\left\{\frac{E[\phi_i+\varepsilon\delta\phi_i]-E[\phi_i]}{\varepsilon}\right\}$. Requiring that the energy is stationary with respect to variations and putting as constraint the fact that the orbitals must be normalized, we get:

$$\delta E = \delta\left[\left\langle \psi \left| \hat{H} \right| \psi \right\rangle - \sum_i \epsilon_i \int d\overrightarrow{r}\, |\phi_i|^2\right] = 0,$$

which yields the Hartree-Fock equation [4]:

$$\left[\hat{T} + V_H + \hat{V_F}\right]\phi_k(\overrightarrow{r}) = \epsilon_k\phi_k(\overrightarrow{r}),$$

where

$$V_H(\vec{r}_1) = \int u(\vec{r}_1,\vec{r}_2)\rho(\vec{r}_2)d\vec{r}_2,$$

is the Hartree potential that depends on the local particle density $\rho(\vec{r}_2)$ and expresses the potential energy of a particle at point $\vec{r}_1$ due to the interaction $u(\vec{r}_1, \vec{r}_2)$ and $\hat{V}_F$ is the Fock operator based on the Fock potential:

$$V_F(\vec{r}_1, \vec{r}_2) = -u(\vec{r}_1, \vec{r}_2)\rho(\vec{r}_1, \vec{r}_2),$$

which depends on the non-local density $\rho(\vec{r}_1, \vec{r}_2)$. Hence, the Hartree term can be written as a potential which is common for all particles, while the Fock term gives in fact rise to slightly different potentials for each particle.

2.1.3 Solving the Hartree-Fock equation

Since both the Hartree and Fock potentials depend on the orbitals $\phi_i(\overrightarrow{r})$, the HF equation derived above is non-linear. Therefore, this equation can only be solved self-consistently using the method of iterations by following the steps that are described below:

1. We start by making an initial guess for the orbitals $\{\phi_i\}_{i=1...n}$.
2. Particle density $\rho_{old}(\overrightarrow{r})$ and particle non-local density $\rho_{old}(\overrightarrow{r}, \overrightarrow{r}')$ can be calculated.
3. From the densities found in step 2 (or 6), we can calculate the potentials: $V_H[\rho(\vec{r})]$ and $V_F[\rho(\overrightarrow{r}, \overrightarrow{r}')]$respectively and build the total Hamiltonian of the system.
4. Keeping V_H and V_F fixed, we can now solve the Hartree-Fock equation:

$$\left[\hat{T} + V_H + \hat{V}_F\right] \phi_k(\overrightarrow{r}) = \epsilon_k \phi_k(\overrightarrow{r}),$$

   which yields new orbitals $\phi_k(\overrightarrow{r})$.
5. Subsequently, the new orbitals yield new densities $\rho_{new}(\overrightarrow{r})$ and $\rho_{new}(\overrightarrow{r}, \overrightarrow{r}')$ respectively.
6. The new densities are used now, after some mixing with the old ones - the reason of this mixing will be explained soon - , as a new input so that we can start again from step 3.

We repeat the described process until convergence is reached. In other words, we continue until the difference between the new and old density is smaller than some chosen tolerance. The most common trick used in order to achieve convergence is to mix the densities from the previous iteration with the new densities obtained from STEP 5 above. An extra step is then added to the method. Hence, after STEP 4 we define (for each iteration m that is performed) the new mixed densities as $\rho_{new} = \alpha\rho^{(m)} + (1-\alpha)\rho^{(m-1)}$, where α is a parameter that determines the amount of mixing.

In order to solve the HF equation in STEP 4, we work in a configuration space based on some arbitrary complete and orthogonal set of single-particle wave functions. The most commonly used set is the harmonic oscillator (HO) wave functions. Thus, each one of the orbitals $\{\phi_i\}_{i=1...n}$ is written as linear combination of these HO wave functions, e.g.

$\phi_1(\overrightarrow{r_1}) = \sum_{i=1}^{N} c_i^1 b_i(\overrightarrow{r_1})$ where N is the number of basis functions that are used for the expansion. The coefficients c_i^j are then determined in such a way that the corresponding energy has a minimum (variational principle). The HF equation is eventually transformed into a matrix eigenvalue equation that can be solved using existing numerical methods.

2.2 Hartree-Fock-Bogoliubov (HFB) method

The procedure of solving the HF equation self-consistently for a system of particles inside a nucleus provides us with a rather satisfactory description of the nuclear charge density distribution. However, in order to be able to understand and describe phenomena experimentally observed, like the spectral energy gap in even-even nuclei, we have to take into account the correlations due to the short-range part of the nucleon-nucleon interaction, called pairing [16]. Thus, by enhancing the HF method we will be capable of laying out an improved description of the nuclear charge density distributions and their properties, i.e. rms (root-mean-square) radii and higher order radial moments.

Pairing correlations are described in the BCS method, developed by the solid-state physicists Bardeen, Cooper and Schrieffer (BCS) in 1957, so that it could be applied to the theory of superconductivity. Later, the same theory was also applied to nuclei by Bohr, Mottelson and Pines in 1958 [13] after they realized that the effect of pair interaction was analogous to the superconductivity in metals. Therefore, using the wave-function suggested by BCS, whose form is demonstrated below, as ansatz (instead of the more simplified Slater determinant) and vary the new wave function to find again the minimum of the energy after having already solved HF equations leads to a more powerful approximation for the description of nuclear many-body systems. Finally, the BCS approximation in turn, constitutes the starting point of the formulation of the Hartree-Fock-Bogoliubov (HFB) method.

2.2.1 BCS approximation

The concept of pairing correlations implies that the motion of nucleons is disturbed by their interactions with other nucleons. Thus, nucleons can be seen as quasi-particles (same undisturbed particles but with different masses). Hence, in the BCS approximation the quasi-particle formalism is used. We look for a more general product of wave functions consisting of independently moving quasi-particles and thus, we make an ansatz different from the Slater determinant that is used in the HF method. The most appropriate ansatz has been proven to be the one analogous to the ground state wave function suggested by Bardeen, Cooper and Schrieffer for determining the ground state of a superconductor. The BCS wave function for nuclei is then illustrated in the following way:

$$\psi_o^{BCS} = \prod_{\nu} (U_\nu + V_\nu \alpha_\nu^+ \alpha_{\overline{\nu}}^+) \left|0\right\rangle ,$$

where $|0\rangle$ is the vacuum state and V_ν, U_ν represent variational parameters. These parameters are subject to the constraint $V_\nu^2 + U_\nu^2 = 1$ due to the normalization condition, since they are regarded as the probability that a certain HF pair state $(\nu, \overline{\nu})$ is or is not occupied respectively. Additionally, according to the variational principle these parameters are determined in such a way that the corresponding energy has a minimum.

In the HF method, a Slater determinant type wave-function is used as ansatz. Given the fact that it represents particles that occupy the orbitals independently, this ansatz is not able to reproduce the desirable results. On the other hand, the BCS wave function provides a more accurate description of the system as it always contains a term with the right number of particles that occupy orbitals in pairs. However, the new ansatz contains also terms with the wrong number of particles. This is well illustrated by considering the simplest case of two existing levels and comparing them to the corresponding two-particle Slater determinant. We consider then a space with two two-fold degenerate levels, called s and r. The solution with the lowest energy is frequently obtained when the particles occupy the lowest levels. Therefore, according to the definition of the Slater determinant in 2.1.1, the wave function for two particles occupying these levels will be given by:

$$\psi(1,2) = \frac{1}{\sqrt{2}}(\phi_s(r_1)\phi_{\overline{s}}(r_2) - \phi_s(r_2)\phi_{\overline{s}}(r_1))$$

or

$$\psi = \alpha_s^+ \alpha_{\overline{s}}^+ \left|0\right\rangle,$$

which in fact represents the independent orbital occupation of two particles s and $\overline{s}$ in the lowest orbital. Thus, the wave-function consists of only one Slater determinant. On the other hand, the BCS wave function represents particles in pairs occupying the orbitals. Hence, for two pairs of particles occupying same, as before, levels s and r, the wave-function takes the form:

$$\psi^{BCS} = (U_r + V_r \alpha_r^+ \alpha_{\overline{r}}^+)(U_s + V_s \alpha_s^+ \alpha_{\overline{s}}^+)\left|0\right\rangle,$$

which can be written:

$$\psi^{BCS} = (\psi_{(0)} + \psi_{(2)} + \psi_{(4)}),$$

where

$$\psi_{(0)} = U_r U_s \left|0\right\rangle,$$
$$\psi_{(2)} = (V_r U_s \alpha_r^+ \alpha_{\overline{r}}^+ + U_r V_s \alpha_s^+ \alpha_{\overline{s}}^+)\left|0\right\rangle,$$
$$\psi_{(4)} = V_r V_s \alpha_r^+ \alpha_{\overline{r}}^+ \alpha_s^+ \alpha_{\overline{s}}^+ \left|0\right\rangle.$$

We then deduce that the first component contains no pairs, the second component contains one pair, which alternatively occupies levels s and r, and the third component describes a situation where both levels are occupied by these two pairs. Therefore, only one of the terms, that is $\psi_{(2)}$, contains the proper quantity of particles. In this case, we need to find the right way to treat the total wave function so that we take as average the right amount of particles. In fact, each component in the expression of the wave function contributes to a particular extent to the description of a system's state. The resulting weighted terms will then reproduce the right number of particles by making use of an additional constraint during the minimization process of the Hamiltonian, using BCS as wave-function.

According to the variational principal we minimize the total ground state energy with respect to all possible choices of the U and V coefficients. However, we minimize the energy by calculating the expectation value of $\hat{H}' = \hat{H} - \lambda\hat{N}$, that is

$$E^{BCS} = \frac{\left\langle \psi^{BCS} \right| \hat{H}' \left| \psi^{BCS} \right\rangle}{\left\langle \psi^{BCS} \mid \psi^{BCS} \right\rangle} = \frac{\left\langle \psi^{BCS} \right| \hat{H} - \lambda\hat{N} \left| \psi^{BCS} \right\rangle}{\left\langle \psi^{BCS} \mid \psi^{BCS} \right\rangle},$$

where λ is a Lagrange multiplier and $\hat{N}$ the number operator defined as:

$$\hat{N} = \sum_{\nu} \left(\alpha_{\nu}^{+} \alpha_{\nu} + \alpha_{\overline{\nu}}^{+} \alpha_{\overline{\nu}} \right),$$

summing over all the pair states $(\nu, \overline{\nu})$. Therefore, the condition that assures that the average number of particles equals the actual number of particles, $\overline{N}$, is represented by $\langle N \rangle = \left\langle \psi^{BCS} \right| \hat{N} \left| \psi^{BCS} \right\rangle = \overline{N}$. Combined with the normalization condition, parameters V_ν and U_ν can now be fully determined.

2.2.2 The HFB approximation

According to the previous subsection 2.2.1, the BCS wave function is used in order to provide a more appropriate representation of nuclear states. Therefore, based on the mean-field that was already found in the HF method we perform again the minimization process of the energy in order to determine parameters V_ν and U_ν for each HF pair state $(\nu, \overline{\nu})$. The Hartree-Fock-Bogoliubov (HFB) method is similar to the BCS method. However, in HFB, during the minimization of the Hamiltonian we minimize with respect to both the V_ν and U_ν coefficients, as well as the orbitals. In this case, the mean-field is also varied.

2.2.3 Solving the HFB equation for spherical and deformed nuclei

The iterative process is also used in the new approximation, and HFB equations are solved using the simple iterative diagonalization method with mixing of orbitals as described in 1.1.3. Hence, same mixing tricks are used in order to facilitate convergence. Moreover, the harmonic oscillator (HO) basis is again used in the HFB method for expanding the single-particle wave-functions of neutrons and protons for a given nuclear state. For A particles and considering the HF-limit, the particle density is written:

$$\rho(\overrightarrow{r}) = \sum_{i}^{A} \left| \phi_i(\overrightarrow{r}) \right|^2 = \sum_{i=1}^{A} \phi^*_{n_i l_i j_i m_i}(\overrightarrow{r}) \phi_{n_i l_i j_i m_i}(\overrightarrow{r}),$$

which is the sum of all individual particle densities for all A particles, with each one of them being in a particular $nljm$ state. Each one of the occupied orbitals $\{\phi_i\}_{i=1...A}$ is a linear combination of the HO wave functions. Using jj-coupling, the particle density can be written as:

$$\rho(\overrightarrow{r}) = \sum_{JM} \rho_{JM}(r) Y_{JM}(\theta, \varphi),$$

meaning that the particle density can finally be written as a superposition of all possible JM quantum states.

For the case of a spherical shell model the sum of the HO wave functions, used as a basis for the calculations, must be spherical. Therefore, we restrict ourselves to spherical symmetry by taking into consideration only the part for which $J = M_J = 0$. In spherical symmetry, the solutions to the HFB equations are provided by HOSPHE (v2.00) which is a new version of the program HOSPHE (v1.02) [7]. On the contrary, in the study of deformed nuclei, l, j and m_j are no longer "good" quantum numbers and consequently spherical symmetry breaks down. Therefore, it is essential to take into account more quantum states for a variety of J

and M_J values, so that the particle density will be a superposition of several JM quantum states. In the case of deformed nuclei, the HFB equations are solved by HFBTHO (2.00d) [22], using the cylindrically deformed HO basis.

2.3 Multiconfiguration Dirac Hartree-Fock method

The Multi-Configuration Dirac-Hartree-Fock (MCDHF) approach is used for the determination of atomic properties. In contrast to nuclear systems where the non-relativistic Schrödinger equation is solved, in atoms it is necessary to make use of a relativistically correct expression for the kinetic energy. The electrons move with relativistic velocities around the nucleus and thus, the relativistic effects play an important role in the determination of their bound states. Hence, the Dirac's equation is solved instead. Furthermore, the wave-functions are now configuration state functions that are formed by angular coupling of the orbitals in an electron configuration. The calculations based on the MCDHF approach are performed with the new version of the GRASP2K relativistic atomic structure package [11].

2.3.1 Solving the relativistic wave equation - Dirac's equation

In nuclear systems, the non-relativistic expression for the Hamiltonian is given by:

$$\hat{H} = \frac{\hat{p}^2}{2m} + \hat{V},$$

and the eigenvalue problem is of the form:

$$\hat{H}\psi(\vec{r}) = (\frac{\hat{p}^2}{2m} + \hat{V})\psi(\vec{r}) = E\psi(\vec{r}),$$

which is the time-independent Schrödinger's equation, where $\psi(\vec{r})$ are the wave-functions describing the system. However, in atomic systems, for the kinetic energy of the electrons we need to use the relativistic expression:

$$(E - V) = \sqrt{(pc)^2 + (m_0c^2)^2},$$

for particles moving under the influence of a potential V. Here, m_0 is the electron's rest mass. Hence, one may postulate:

$$(H - V)^2\psi = (-i\hbar c\nabla)^2\psi + (m_0c^2)^2\psi.$$

According to Dirac, Schrödinger's equation for spin-$\frac{1}{2}$ particles can take the form:

$$H\Psi = \sqrt{-(\hbar c)^2\nabla^2 + (m_0c^2)^2}\Psi + V\Psi,$$

where Ψ is a column matrix or spinor:

$$\Psi(\vec{r}) = \begin{bmatrix} \psi_1(\vec{r}) \\ \psi_2(\vec{r}) \\ \psi_3(\vec{r}) \\ \psi_4(\vec{r}) \end{bmatrix},$$

with the wave-functions ψ representing respectively spin-up and spin-down states of a particle, as well as spin-up and spin-down states of the corresponding antiparticle. It can then be shown that the Dirac-Coulomb Hamiltonian can be written as:

$$H_{DC}\begin{pmatrix}\psi_1\\ \psi_2\\ \psi_3\\ \psi_4\end{pmatrix} = c(\vec{\alpha}\vec{p}+\beta m_0 c)\begin{pmatrix}\psi_1\\ \psi_2\\ \psi_3\\ \psi_4\end{pmatrix} + V_C\begin{pmatrix}\psi_1\\ \psi_2\\ \psi_3\\ \psi_4\end{pmatrix},$$

where $\vec{\alpha}\vec{p} = \begin{pmatrix} 0 & 0 & p_z & p_x - ip_y \\ 0 & 0 & p_x + ip_y & -p_z \\ p_z & p_x - ip_y & 0 & 0 \\ p_x + ip_y & -p_z & 0 & 0 \end{pmatrix}$ and $\beta = \begin{pmatrix} 1 & 0 & 0 & 0 \\ 0 & 1 & 0 & 0 \\ 0 & 0 & -1 & 0 \\ 0 & 0 & 0 & -1 \end{pmatrix}$. The eigenvalue problem then takes the form:

$$(E - V_C)\begin{pmatrix}\psi_1\\ \psi_2\\ \psi_3\\ \psi_4\end{pmatrix} = c\begin{pmatrix} m_0c & 0 & p_z & p_x - ip_y \\ 0 & m_0c & p_x + ip_y & -p_z \\ p_z & p_x - ip_y & -m_0c & 0 \\ p_x + ip_y & -p_z & 0 & -m_0c \end{pmatrix}\begin{pmatrix}\psi_1\\ \psi_2\\ \psi_3\\ \psi_4\end{pmatrix}$$

This is a set of four simultaneous, partial differential equations that needs to be solved in order to obtain all the components of the energy eigenfunctions $\psi(\vec{r})$. However, two of these eigenfunctions correspond to antiparticle states that are states of negative energy and they are of less significance in our calculations. Since no transition between positive and negative energy states occurs, the negative energy states can be neglected.

2.3.2 Multiconfiguration approach

In the previous section, we discussed Dirac's equation that solves the relativistic wave function, establishing spin s as an additional degree of freedom for elementary particles, like electrons. Hence, the spin of the electrons will now be coupled to their orbital angular momentum l, so that their total angular momentum is given by $j = l + s$.

In n-electron systems, the Dirac-Coulomb Hamiltonian is given by:

$$\hat{H}_{DC} = \sum_{i=1}^{n}[c(\vec{\alpha}\vec{p}+\beta m_0 c) + V_i^N] + \frac{1}{2}\sum_{i\neq j}^{n}\frac{1}{|r_i - r_j|},$$

where the Coulomb potential between two electrons: $\sum_{i\neq j}^{n}\frac{1}{|r_i - r_j|}$ corresponds to the potential produced due to the two-particle interaction, generally expressed as $\frac{1}{2}\sum_{i\neq j}^{n}u(\vec{r_i},\vec{r_j})$ in 2.1.1. In the expression above V_i^N is the electron-nucleus Coulomb interaction, which in the case of a point-like nucleus reduces to $V_i^N = -\frac{Z}{r_i}$. However, assuming an extended charge distribution V_i^N may be slightly different for two isotopes which ultimately causes the field shift between analogue transitions in an isotope pair. According to the mean-field approximation, the Hamiltonian of the many-electron system then reduces to the Dirac-Hartree-Fock (DHF) Hamiltonian:

$$\hat{H}_{DHF} = c(\vec{\alpha}\vec{p} + \beta m_0 c) + V_i^N + V_H + \hat{V}_F,$$

Due to the spherically symmetric charge distribution of the electrons, it is radially symmetric. Therefore, only the radial part of the Hamiltonian is the one that must be calculated through a self-consistent field procedure similar to the one described in 2.1.3.

In order to estimate the potential $V_H + \hat{V}_F$, we have to find approximate electron wave functions for the atomic states. A single Slater determinant (see 2.1.1) is not necessarily an eigenfunction of the atomic system and therefore linear combinations of determinants are used instead. These linear combinations are called configuration state functions (CSFs) and they are denoted as $\Phi(\gamma PJM_J)$, where γ represents the electron configuration. The notation indicates that the CSFs are state functions with the same parity P, total angular momentum J and component M_J along the z-direction. Finally, the atomic state functions (ASFs) Ψ will be a so-called multiconfiguration expansion over the CSFs, so that we can write:

$$\Psi(\gamma PJM_J) = \sum_{i=1}^{N} c_i \Phi(\gamma_i PJM_J),$$

where c_i are referred to as mixing coefficients with $\sum_{i=1}^{N} c_i^2 = 1$. The most appropriate wave function Ψ, which describes a state of the given system, is obtained through an optimization process by applying the variational principle (see 2.1.2). The expression for the approximate state energy will now be:

$$E(\gamma PJM_J) = \sum_{i=1}^{N}\sum_{j=1}^{N} c_i c_j \left\langle \Phi(\gamma_i PJM_J) \left| \hat{H} \right| \Phi(\gamma_j PJM_J) \right\rangle.$$

The mixing coefficients then need to be determined, based on the argument that the energy is stationary with respect to variations. This process finally yields a set of coupled differential equations that are similar to the HF equations, which need again to be solved iteratively until convergence is reached (see 2.1.3).

3 Validation of nuclear interaction

The main purpose of this section is to demonstrate the validity of the nuclear interaction based on the selected Skyrme-type forces and to investigate which set of parameters is the most appropriate. For that reason, the nuclear charge density distributions are calculated for a variety of isotopes and compared to the experimental data, already obtained in 1987, from elastic electron scattering experiments [25]. Having obtained the best possible description of the charge density distributions, it is then feasible to determine fundamental properties of the atomic nucleus, like the rms charge radii, which, together with higher radial moments values, give a satisfactory measurement of its size and shape.

The determination of nuclear properties constitutes a fundamental part of nuclear physics, but it seems to effect at a particular extent atomic physics, too. Phenomena observed, like the small shift in atomic energy levels and transitions among different isotopes, are due to

the differences in mass and size, as well as the shape differences of the nuclear charge density distributions. Therefore, it is of great importance to achieve the best possible description of the nuclear systems in order to predict the effect on isotope field shifts in atoms (see Chapter 4). For comparison, higher order radial moments are also calculated for a two-parameter Fermi distribution. Thus, we can compare the radial moments resulting from the more realistic HFB distributions with the ones resulting from the simplified Fermi distribution. The actual purpose of this procedure is to be able to finally compare the effect that these two, slightly different, distributions have on the field shifts that are being investigated throughout the next two chapters.

3.1 Background

The forces acting between the nucleons give rise to an average single-particle potential according to the mean-field methods. The form of the potential term of the Hamiltonian, then depends on the choice of the interaction. Since it is impossible to microscopically calculate the interactions between nucleons, especially for the case of heavy nuclei, the only way is to use phenomenological forces that contain a certain number of parameters. By adjusting these parameters, we try to reproduce as many experimental data as we can. The Skyrme interaction is a phenomenological effective nucleon-nucleon interaction that is applicable to many-body methods and seems to be the fastest one when we solve HF or HFB equations by using numerical methods.

In order to formulate the effective nucleon-nucleon interactions, we require the translational and rotational symmetries, exchange of coordinate invariance etc. to be fulfilled [17]. Moreover, the four possible ways -depending on the spin component- that protons and neutrons interact with each other, as well as the spin-orbit interaction, must be taken into consideration in the expression for the potential. Lastly, even if the two-body forces are the strongest inside the nucleus, a three-body term is included and provides an enhanced description of the nuclear model. Therefore, the Skyrme interaction potential contains a two- and a three-body term, as it is shown below:

$$V = \sum_{i<j} V(i,j) + \sum_{i<j<k} V(i,j,k),$$

where the two- and three-body terms are respectively:

$$V(1,2) = t_0(1 + x_0 P^\sigma)\delta(\overrightarrow{r_1} - \overrightarrow{r_2}) +$$

$$+\frac{1}{2}t_1[\delta(\overrightarrow{r_1} - \overrightarrow{r_2})\overrightarrow{k^2} + \vec{k}^2\delta(\overrightarrow{r_1} - \overrightarrow{r_2})] + t_2\vec{k}\delta(\overrightarrow{r_1} - \overrightarrow{r_2})\vec{k} +$$

$$+iW_0(\vec{\sigma}^{(1)} + \vec{\sigma}^{(2)})\vec{k} \times \delta(\overrightarrow{r_1} - \overrightarrow{r_2})\vec{k},$$

where $\vec{k} = \frac{1}{2i}(\nabla_1 - \nabla_2)$ is the operator of the relative momentum, and:

$$V(1,2,3) = t_3\delta(\overrightarrow{r_1} - \overrightarrow{r_2})\delta(\overrightarrow{r_2} - \overrightarrow{r_3})$$

The short range expansion of the two-body term (that is used to simplify the calculations) and the zero-range force that has been assumed for the three-body term contain a certain number of parameters, i.e. t_0, t_1, t_2, t_3, x_0 and W_0, adjusted to reproduce the experimental data that has been adopted. In many Skyrme parametrizations the original three-body force is often

replaced by a density-dependent two-body interaction which makes the method similar to density functional theory. In addition, the mathematical form of this force is extremely simple, as it includes δ-functions that can simplify the calculations to a great extent, and as a consequence make them fast enough [18].

3.2 Method

Two different sets of parameters have been selected for the theoretical calculations of the nuclear charge density distributions. These are called SLY4 and UDF1. In order to check the range of validity of these two parametrizations of Skyrme interactions, we made a comparison of theoretical and experimental charge distributions. This comparison concerns the proton densities of the selected nuclei, since these are the only ones that can be measured experimentally.

3.2.1 Folding of proton density

The initial calculations were carried out assuming that protons are point particles. Hence, an initial representation of proton densities inside various nuclei was obtained. However, protons are composite particles, made of quarks. In order to achieve a more accurate description of the charge density distributions, we "folded" the proton densities using the convolution formula:

$$\varrho_c(\vec{r}) = \int d^3\vec{r'}\rho_p(\vec{r'})g(\left|\vec{r} - \vec{r'}\right|),$$

where $\rho_p(\vec{r})$ is the initially calculated proton density and

$$g(\vec{r}) = (r_0\sqrt{\pi})^{-3}e^{-(\vec{r}/r_0)^2},$$

the form factor, which is assumed a Gaussian with $r_0 = \sqrt{\frac{2}{3}}\langle r_p\rangle_{rms}$ [6]. Since the proton radius determination experiments have resulted in different values, it is essential to use a proton radius value that is more realistic. Experiments based on electron scattering measurements have displayed proton radius $\langle r_p\rangle_{rms} = 0.88$ fm [19]. On the other hand, in experiments where muonic hydrogen was used the radius was found to be $\langle r_p\rangle_{rms} = 0.84$ fm [15]. Of course, a physical parameter can not depend on the method of extraction. Hence, until the proton radius puzzle is finally solved we performed the calculations by assuming $\langle r_p\rangle_{rms} = 0.88$ fm. However, later in the results the case of folding for a different proton radius value is compared, so that we can draw further conclusions of the effect of the proton size in the folding process.

The effect of folding, for each one of the sets of parameters, is separately shown in Figure 3.1 for the SLY4 parameter set and in Figure 3.2 for the UDF1 parameter set. The "old" proton densities and the "folded" nuclear charge density distributions are compared with the corresponding experimental charge density for some chosen elements. In order to make the comparison with the experimental curve easier and at the same time highlight the effect of convolution to the proton densities, we plotted the logarithm of the proton density values against the radius r measured in fermi (fm).

Considering the four different nuclei illustrated, we deduce that the "folded" proton densities (in black for SLY4 and green for UDF1), for both sets of parameters, are smeared out

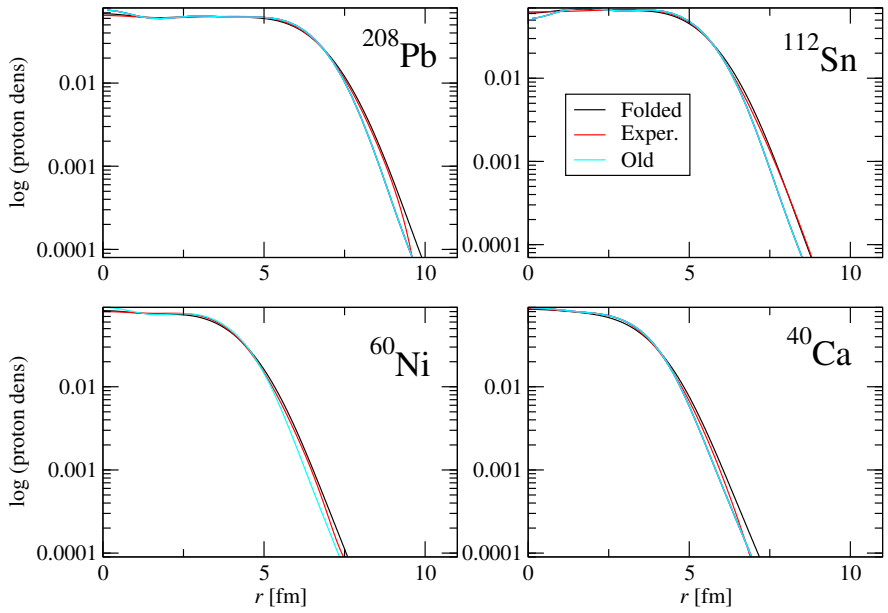

Figure 3.1: Comparison of experimental data with theoretically calculated nuclear charge density distributions for several isotopes using the SLY4 set of parameters. The curve labeled "Old" corresponds to the charge density assuming point-like protons. For the curve labeled "Folded" the quark structure of the protons is taken into account by a folding method using $\langle r_p \rangle_{rms} = 0.88$ fm.

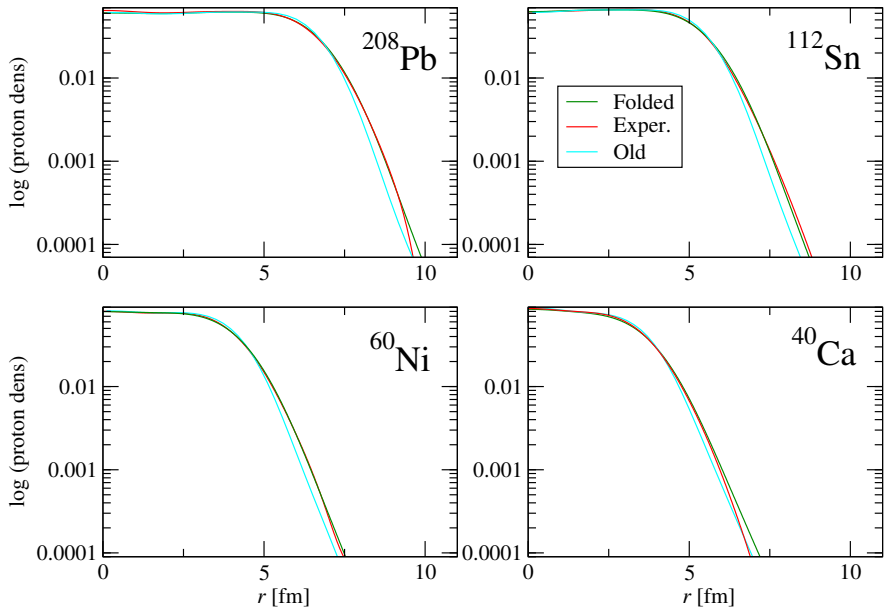

Figure 3.2: Same as Figure 3.1 but for the UDF1 set of parameters.

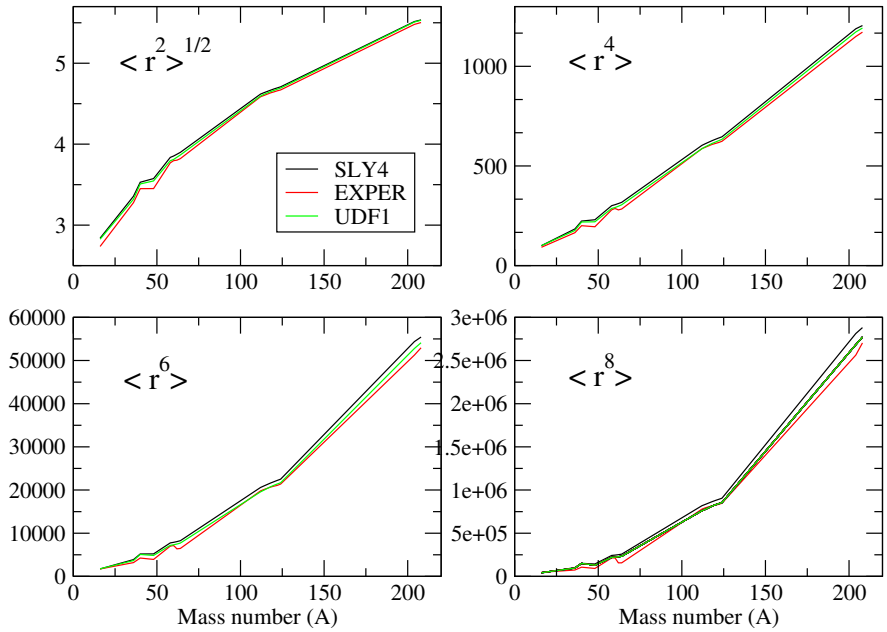

Figure 3.3: rms and r^4, r^6 and r^8 moments of the calculated charge distributions are compared to the experimental data. The moments $\langle r^N \rangle$ are calculated after folding, using $\langle r_p \rangle_{rms} = 0.88$ fm.

as we expected, and as a consequence they overall approach more the experimental (in red) charge density distributions. In some cases, the theoretical distributions present an almost perfect match to the corresponding experimental distributions. Thus, by taking into account the real nature of protons, the density distributions display a longer "tail" that at a great extent improves the theoretical predictions.

3.2.2 Comparison of the theoretical models

After having performed the folding of the proton densities, we are now in position to compare the two parametrizations, SLY4 and UDF1, with the experimental measurements. Thus, we will then be able to decide which set provides the most reliable description of the nuclear charge density distributions. Since the approximation for the electron density distribution that we are interested in (see chapter 4) is based on a polynomial expansion of even r^N moments of the nuclear charge density distribution, a more systematic comparison of the two Skyrme-parameter sets is necessary. Therefore, the rms radii are compared together with the moments for r^4, r^6 and r^8, for 16 spherical isotopes of 6 different elements: Pb, Sn, Ni, Ca, S and O. The results are displayed in a set of plots in Figure 3.3, where the rms and moments are plotted for different mass numbers A.

As seen in Figure 3.3, the two theoretical models exhibit slightly different plots. For a few cases (mostly for light isotopes), both interactions seem to represent the experimental data equally well, however, overall the UDF1 interaction gives a better description of all four moments. Especially for the cases of the tin isotopes, that is $A = 112 - 124$, the rms radii given from UDF1 are significantly closer to the ones experimentally measured. Additionally, the higher order moments for the same isotope cases present an almost perfect match. For the heavy lead isotopes, that is $A = 208 - 210$, although the UDF1 curve displays an observable

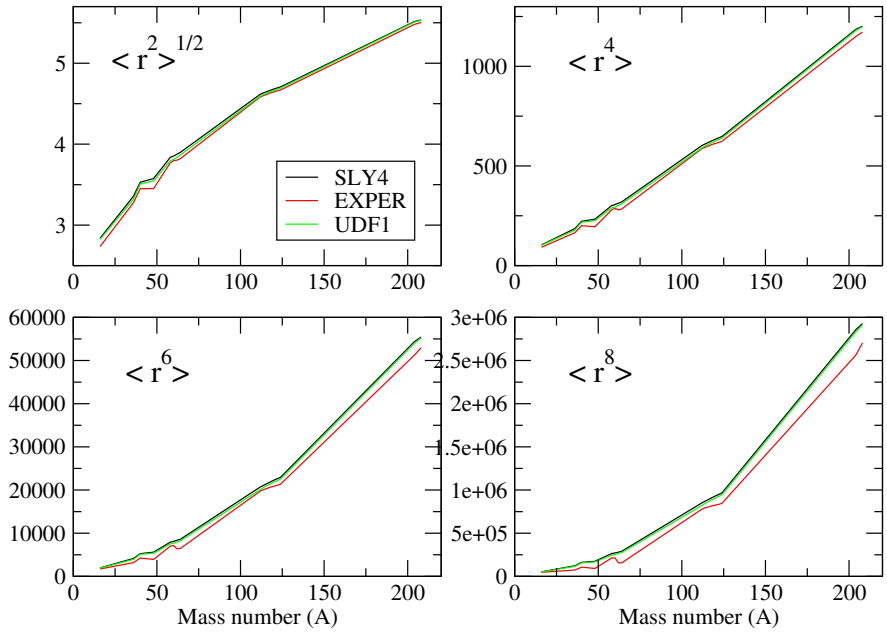

Figure 3.4: rms and r^4, r^6 and r^8 moments, calculated based on the Fermi distribution model, are compared to the experimental data.

difference from the experimental one, it keeps representing better the values than the curve resulting from the SLY4 model. Lastly, observing all four plots at the same time we can deduce that the higher the order of the calculated moment is, the more the UDF1 interaction becomes appropriate.

In calculations of electron states in atoms, the nucleus is often approximated as a Fermi distribution. In this way, one may take into account that the nucleus is not a point-like particle and obtain a more realistic potential for the electrons. In such a model, the Fermi distribution approximating the nuclear charge distribution takes the form:

$$\rho(r) = \frac{\rho_0}{1 + e^{\frac{(r-c)}{\alpha}}},$$

which is a spherical two-parameter model. The parameter α is given by the relation:

$$t = 4\ln(3)\alpha,$$

where t is the skin thickness of the distribution. The skin thickness is defined as the interval where the density is decreased from 90% to 10% of $\rho(0)$ and it is assumed to have a constant value $t \simeq 2.3$ fm. The parameter c determines the size of the nucleus. Lastly, the value of ρ_0 is determined by the normalization condition:

$$4\pi \int \rho(r) r^2 dr = 1.$$

In order to compare our realistic and microscopically calculated charge distributions to those of the Fermi distribution model, we fit the c-parameter so that both distributions have the same $\langle r^2 \rangle$ values. We may then compare the higher moments to see if these can be accurately

described by the Fermi distribution. The results are displayed in Figure 3.4. Although the $\langle r^2 \rangle$ values are identical to the ones from the realistic HFB calculations, they are again shown in this figure.

As seen in Figure 3.4, the use of different rms radii values (based on the SLY4 and UDF1 calculations respectively) do not result in observable differences in the values of the higher order moments, once the Fermi model is used in both cases to calculate them. Hence, the black and green curves are almost identical in the $\langle r^4 \rangle$-, $\langle r^6 \rangle$- and $\langle r^8 \rangle$-moment plots. Comparing Figure 3.4 to Figure 3.3, we deduce that the higher moments described by the Fermi distribution present a larger difference from the experimental curve than the ones predicted by the realistic SLY4 and UDF1 models. Therefore, the Fermi approximation of the nuclear charge density distributions cannot represent the experimental data equally well, especially when it comes to the r^6 and r^8 higher moments.

3.3 Accuracy of theoretical models

In this subsection we discuss the validity of the Skyrme nuclear interactions by demonstrating their relative, to the experimental values, errors ($R.E.$) of rms radius, as well as r^4, r^6 and r^8 moments. These are given by:

$$R.E. = \frac{\left\langle r^N_{theor} \right\rangle - \left\langle r^N_{exp} \right\rangle}{\left\langle r^N_{exp} \right\rangle} = \frac{\Delta \left\langle r^N \right\rangle}{\left\langle r^N_{exp} \right\rangle},$$

for $N = 2, 4, 6$ and 8 respectively. These errors are calculated for both the realistic HFB and Fermi distributions and are discussed in subsections 3.3.1 and 3.3.2, respectively. In addition, the rms values of these relative errors:

$$R.E._{rms} = \sqrt{\frac{1}{K}\left[\sum_{i=1}^{K}\left(\frac{\left\langle r^N \right\rangle_i - \left\langle r^N_{exp} \right\rangle_i}{\left\langle r^N_{exp} \right\rangle_i}\right)^2\right]}$$

have been calculated for all moments of both interactions and are also presented. K is the total number of the isotopes studied, that is $K = 16$. Hence, a comparison between the SLY4 and UDF1 models can easier be carried out.

Lastly, the mean value of the errors for the rms radii can be compared to the corresponding rms values of the typical experimental uncertainties [25]. The $(R.E._{RMS})_{exp}$ are indicatively calculated for the Pb and Ni isotopes. In subsection 3.3.3, the effect of the folding procedure for different proton radius values is discussed and thus, conclusions can be drawn about the effect of proton radius measurements on the calculations of nuclear charge density distributions.

3.3.1 The realistic HFB models

Although a comparison between theoretical models and experimental measurements has already been performed in subsection 3.2.2, a quantitative analysis is also provided here in order to highlight the appropriateness of the UDF1 set of parameters. As seen in Figure 3.5, the calculated errors for the values based on the UDF1 model are always smaller than the ones based on the SLY4. This is valid for all four moments. Moreover, this allegation

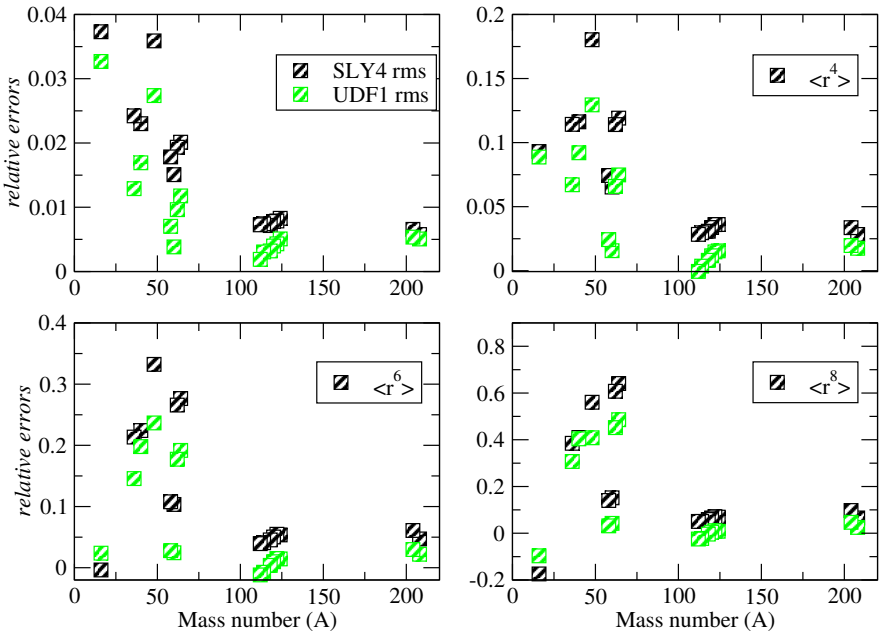

Figure 3.5: Relative errors to the experimental values for the SLY4 and UDF1 theoretical models.

$\langle r_p \rangle_{rms} = 0.88$ fm	SLY4	UDF1
rms	0.01862	0.01300
r^4	0.08404	0.05576
r^6	0.15718	0.10858
r^8	0.30818	0.23463

Table 1: The rms value of the relative errors for rms and r^4, r^6 and r^8 moments of both SLY4 and UDF1 theoretical models.

is confirmed by the calculations of the $R.E._{rms}$ for all the isotopes taken into consideration, illustrated in Table 1 . Interesting to note that in the tin-region, between $A = 112$ and 124, the relative errors are remarkably small for both models. However, UDF1 keeps providing a better representation of the experimental data for all isotopes studied.

Given the typical experimental uncertainties for the measured rms radii of Pb and Ni isotopes, we estimated $(R.E._{rms})_{exp} \simeq 0.0004$ and $\simeq 0.0051$ respectively. We indicatively chose the measurements with the smallest and largest typical uncertainties, so that: $0.0004 \lesssim (R.E._{rms})_{exp} \lesssim 0.0051$. Meaning that the experimental measurements provide, in general, sufficiently accurate results. However, for some isotopes the experimental curve dies unexpectedly fast (see e.g. ^{40}Ca in Fig. 3.1 and 3.2), which is due to the insufficient accuracy of the experimental data for large radii. Eventually, in Figure 3.5 the relative errors are seen to be large for these isotopes and as a consequence the rms value of the errors in Table 1 appears to be increased. This is more pronounced for the higher moments r^6 and r^8. In order to avoid the effect that inaccurate experimental data have on the evaluation of the theoretical models, an alternative error analysis could further be provided with the median values of the relative errors to be given instead.

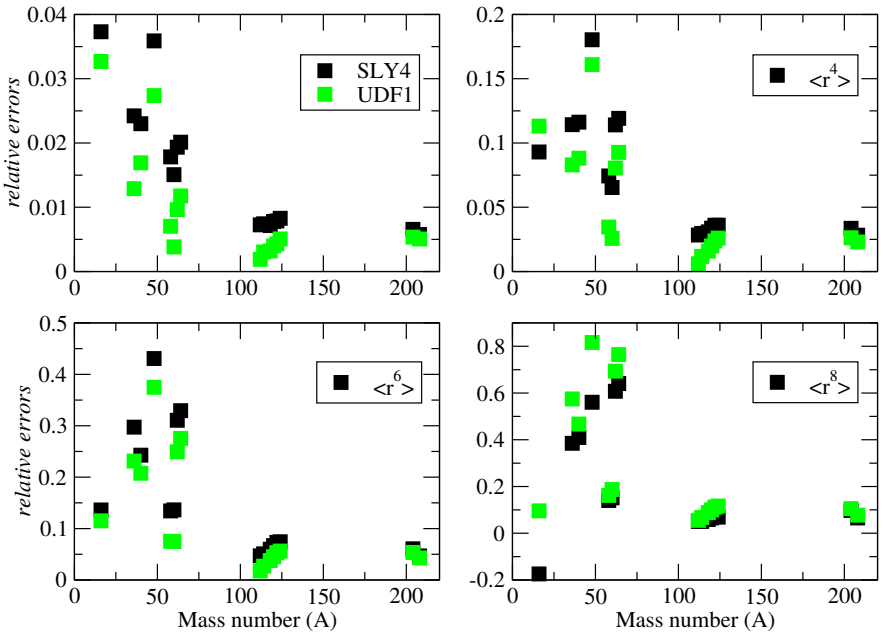

Figure 3.6: Relative errors to the experimental values for the r^4, r^6 and r^8 moments calculated for the Fermi distribution model, based on the SLY4 and UDF1 rms radii values.

	SLY4	UDF1
rms	0.01862	0.01300
Fermi r^4	0.09111	0.06782
Fermi r^6	0.19729	0.16100
Fermi r^8	0.44358	0.38891

Table 2: The rms value of the relative errors for the rms of SLY4 and UDF1 theoretical models and the r^4, r^6 and r^8 moments of the Fermi distribution model.

3.3.2 The Fermi model

As expected (already observed in Fig. 3.4), Figure 3.6 shows that for both interactions the relative errors of the moments described by the Fermi distribution model are larger compared to the ones resulting from the realistic theoretical models UDF1 and SLY4 (see Fig. 3.5 and Table 1). This is also illustrated in the calculations of the averaged errors shown in Table 2. By comparing Table 2 with Table 1, we can conclude that the larger the order of the moment is, the more the averaged value of the errors increases when the Fermi model is being used. The most interesting point here is that the errors of the moments based on the UDF1 rms radii values are the ones that have been increased the most. For the case of the r^8 moment for instance, $(R.E._{rms})_{Fermi} = 0.3889$ is almost twice the $(R.E._{rms})_{Realistic} = 0.2346$. Thus, the r^4, r^6 and especially the r^8 moment are not described as accurate as with the Fermi model and this is most pronounced for the UDF1 parameter set, which was the most appropriate choice. We can then deduce that the choice of a realistic rms radius value for a nuclear charge density distribution does not necessarily result in a precise enough prediction of its higher

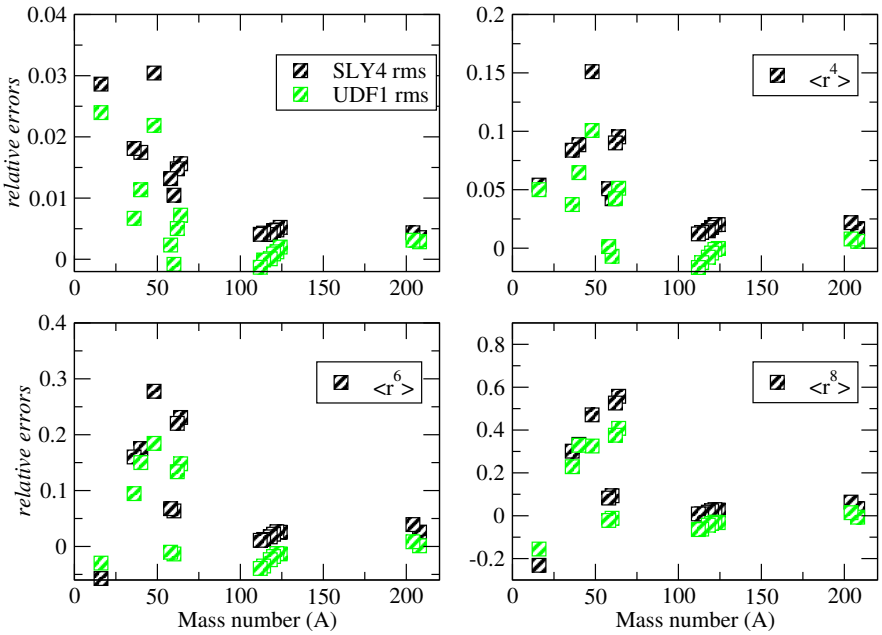

Figure 3.7: Relative errors to the experimental values for the SLY4 and UDF1 theoretical models, folded using a proton radius value $\langle r_p \rangle_{rms} = 0.8$ fm.

moments by the Fermi model.

3.3.3 The effect of folding

As we already saw in subsection 3.2.1, the theoretical considerations of proton density distributions are remarkably improved after taking into account the real nature of the particles. This improvement was achieved by following the described folding procedure using a proton radius value $\langle r_p \rangle_{rms} = 0.88$ fm. Nonetheless, the proton radius has not been confidently determined yet. It is essential then to perform the folding process using a different proton radius value, that is $\langle r_p \rangle_{rms} = 0.8$ fm, and look into the effect of folding in detail. Thus, we will be in position to provide an estimate of how important is, for the theoretical predictions of proton density distributions, to obtain a well determined proton radius value.

An equivalent quantitative analysis as in subsection 3.3.1 is provided here. As seen in Figure 3.7, the relative errors are mainly positive -as it was when $\langle r_p \rangle_{rms} = 0.88$ fm had been used- which means that the theoretically predicted moments are still generally larger than the experimental ones. As already seen in Figure 3.1, the effect of folding is to move the density from the interior to the surface of the nucleus and this increases the radial moments slightly beyond their experimental values. Using a smaller $\langle r_p \rangle_{rms}$ value, as done in Fig. 3.7 and Table 3, leads to a better agreement with experiment (we note here that $\langle r_p \rangle_{rms} = 0$ corresponds to no folding). However, by comparing Tables 1 and 3 one notes that modifying $\langle r_p \rangle_{rms}$ within the range of realistic values has a marginal effect on the results. Other parts of the nuclear model must therefore be improved in order to obtain an even better description of the experimental charge distributions and in particular, the higher order radial moments.

From the comparison between the two Skyrme-parametrizations, SLY4 and UDF1, we

$\langle r_p \rangle_{rms} = 0.8$ fm	SLY4	UDF1
rms	0.01431	0.00914
r^4	0.06352	0.03815
r^6	0.12545	0.08309
r^8	0.26071	0.19562

Table 3: The rms value of the relative errors for rms and r^4, r^6 and r^8 moments of both SLY4 and UDF1 theoretical models, folded for a proton radius value $\langle r_p \rangle_{rms} = 0.8$ fm.

conclude that the UDF1 interaction gives the best description of the radial moments. For $\langle r^2 \rangle^{1/2}$ and the most important moment r^4, we obtain average errors of 1.3% and 5.6%, respectively. In the following chapters, we will use the UDF1 results when calculating the atomic levels.

4 Atomic isotope shift

Nuclear radii have a considerably small size compared to the scale of the atomic structure. However, their finite masses and extended charge distributions have a measurable effect on atomic spectra. Accordingly, the observed analogue atomic spectral lines from different isotopes display a small shift in energy. This is due to the so-called isotope shift (IS), which can be decomposed into the mass shift (MS) and the field shift (FS). The observed IS arises from the difference in energy of the analogue atomic levels i between two isotopes A and A', namely the level isotope shift, which is expressed as:

$$\delta E_{i,IS}^{A,A'} = E_i^{A'} - E_i^A = \delta E_{i,MS}^{A,A'} + \delta E_{i,FS}^{A,A'}.$$

For a particular atomic transition k between upper u and lower l levels, the difference in frequency for a pair of isotopes, namely the frequency isotope shift, is expressed as:

$$\delta \nu_{k,IS}^{A,A'} = \nu_k^{A'} - \nu_k^A = \delta \nu_{k,MS}^{A,A'} + \delta \nu_{k,FS}^{A,A'} = \frac{\delta E_{u,IS}^{A,A'} - \delta E_{l,IS}^{A,A'}}{h}.$$

4.1 Mass shift

The mass shift (MS) effect arises from the finite and different nuclear masses of different isotopes of an element. The mass shift for an atomic level i results from the contribution of the normal mass shift (NMS) and -for atoms with more than one electron- the specific mass shift (SMS). Therefore, the level mass shift is generally described as:

$$\delta E_{i,MS}^{A,A'} = \delta E_{i,NMS}^{A,A'} + \delta E_{i,SMS}^{A,A'} = \frac{K_{MS}^i}{M} - \frac{K_{MS}^i}{M'},$$

or equivalently:

$$\delta E_{i,MS}^{A,A'} = (\frac{M' - M}{MM'}) K_{MS}^i = (\frac{M' - M}{MM'})(K_{NMS}^i + K_{SMS}^i),$$

where M and M' are the atomic masses of the isotopes and K^i_{NMS}, K^i_{SMS} the mass-independent, nuclear recoil normal and specific mass shift parameters [14] [24] [21]. The corresponding line frequency isotope mass shift can then be written as:

$$\delta\nu^{A,A'}_{k,MS} = \delta\nu^{A,A'}_{k,NMS} + \delta\nu^{A,A'}_{k,SMS},$$

with

$$\delta\nu^{A,A'}_{k,MS} = (\frac{M' - M}{MM'})\frac{\Delta K_{MS}}{h} = (\frac{M' - M}{MM'})\Delta\tilde{K}_{MS},$$

where $\Delta K_{MS} = \Delta K_{NMS} + \Delta K_{SMS}$. Now, $\Delta K_{MS} = (K^u_{MS} - K^l_{MS})$ constitute the frequency mass parameters for a transition k that connects the upper u and lower l level. The normal and specific mass shift parameters are provided by the program ris3u [12] included in the GRASP2K package. Hence, together with available nuclear mass data, isotope-dependent energies and total isotope mass shifts are determined. The mass shift effect is dominant in light systems, whereas in heavier systems its contribution becomes smaller.

4.2 Field shift

The isotope field shift (FS) arises from the differences in the nuclear charge density distribution between isotopes, which is caused by the different number of neutrons. Unlike point-like charge distributions, realistic charge distributions alter the central field that the bound atomic electrons experience. Hence, the extended charge distributions influence the presence of the electrons inside the nuclear volume by pulling them out. The electron energy levels and very likely the transition energies will then be affected. Evidently, the effect of the nuclear distributions will be more pronounced for the electrons moving in s and p orbitals. Moreover, the heavier the nuclear systems are, the more the electrons are pulled out and the greater the FS becomes.

4.2.1 Variational approach

In the GRASP2K package [11], the multi-configuration Dirac-Hartree-Fock (MCDHF) method provides an approximate solution of the atomic wave-functions. This method is the so-called variational approach (VA), based on the minimization process of the total energy of the system according to the variational principle (see chapter 2). Since in these calculations the nucleus is assumed to have infinite mass, there is no MS effect contribution. Therefore, by performing separate MCDHF calculations for two isotopes A and A' with different parameter set describing the respective charge distributions, the level field shift of an atomic level i is calculated as:

$$\delta E^{A,A'}_{i,FS} = E^{A'}_i - E^A_i,$$

and consequently, the frequency transition field shift for a certain transition k will be given by:

$$\delta\nu^{A,A'}_{k,FS} \equiv \nu^{A'}_k - \nu^A_k = \frac{\delta E^{A,A'}_{k,FS}}{h},$$

where the difference $\delta E^{A,A'}_k = \delta E^{A,A'}_u - \delta E^{A,A'}_l$ is called transition field shift between the chosen, upper u and lower l, levels. This method is highly model-dependent, since the shape of the nucleus is approximated by a spherical two-parameter Fermi model (see subsection 3.2.2)

in GRASP2K. Namely, the higher than r^2 moments that determine the shape of the nuclear charge distribution are predicted by a Fermi distribution having a diffuseness parameter $t = 2.3$ fm and a radius parameter c tuned to reproduce the desired $\langle r^2 \rangle$ moment. However, the implementation of MCDHF provides the "exact" method for estimating the frequency field shifts, serving as a benchmark when comparing to different perturbative approaches below.

4.2.2 Perturbative methods

As seen in 4.2.1, the "exact" level field shifts are obtained by subtracting one atomic level energy from another, which results in a tiny difference compared to the magnitude of the undisturbed level energies E_i. Therefore, an alternative approach based on the first-order perturbation theory may be used, so that the first-order level field shift of a level i can be written as:

$$\delta E_{i,FS}^{(1)A,A'} = -\int_{R^3} [V_{A'}(\vec{r}) - V_A(\vec{r})]\rho_i^e(\vec{r})d^3\vec{r},$$

where $V_A(\vec{r})$ and $V_{A'}(\vec{r})$ are the one-electron potentials arising from the different nuclear charge distributions for the two isotopes A and A' and $\rho_i^e(\vec{r})$ is the electron density distribution within the nuclear volume of the reference isotope A. In the theoretical considerations of frequency field shifts, it is often assumed that the electron density is constant within the nucleus, that is $\rho_i^e(\vec{r}) = \rho_i^e(0)$. The level and frequency field shifts can then roughly be estimated as:

$$\delta E_{i,FS}^{(1)A,A'} \approx \frac{2\pi}{3} Z\rho_i^e(0)\delta \left\langle r^2 \right\rangle^{A,A'} = F_{i,1}\delta \left\langle r^2 \right\rangle^{A,A'}$$

and

$$\delta \nu_{k,FS}^{(1)A,A'} \approx \frac{Z}{3\hbar}\Delta\rho_k^e(0)\delta \left\langle r^2 \right\rangle^{A,A'} = F_{k,1}\delta \left\langle r^2 \right\rangle^{A,A'},$$

where $\Delta\rho_k^e(0) = \rho_u^e(0) - \rho_l^e(0)$ and $F_{i,1}, F_{k,1}$ are the so-called electronic factors. Thus, the field shift depends only on the difference between the second radial nuclear moments of the chosen pair of isotopes.

This approximation works well as long as the atomic number is not too large. However, in heavier systems, a reformulation of the field shift is needed, where the shape of the electron density inside the nucleus is taken into account. Assuming extended nuclear charge distributions, it can be shown that the electron density to a very good approximation can be expanded, around $r = 0$, as an even polynomial function:

$$\rho_i^e(\vec{r}) \approx b(r) = b_{i,1} + b_{i,2}r^2 + b_{i,3}r^4 + b_{i,4}r^6,$$

so that the first-order level field shift is given by the expansion [12] [20] [5] [10]:

$$\delta E_{i,FS}^{(1)A,A'} = \sum_{N=1}^{4} F_{i,N}\delta \left\langle r^{2N} \right\rangle^{A,A'},$$

where the level electronic factors now are $F_{i,N} = \frac{2\pi}{N(2N+1)} Z b_{i,N}$ for a certain atomic number Z and $\delta \left\langle r^{2N} \right\rangle^{A,A'} = \left\langle r^{2N} \right\rangle^{A'} - \left\langle r^{2N} \right\rangle^{A}$ are the differences of the nuclear radial moments, of

order $2N$ for $N = 1, 2, 3$ and 4, for isotopes A, A'. Accordingly, the first-order frequency field shift will be given by:

$$\delta\nu_{k,FS}^{(1)A,A'} = \sum_{N=1}^{4} F_{k,N}\delta\left\langle r^{2N}\right\rangle^{A,A'},$$

where $F_{k,N} = \frac{1}{\hbar N(2N+1)} Z\Delta b_{k,N}$ are the frequency electronic factors, related to the change in the electronic density inside the nucleus, with $\Delta b_{k,N} = b_{u,N} - b_{l,N}$ defining the difference of the polynomial function coefficients between the upper u and the lower l level.

The electron density $\rho^e(\vec{r})$ is constructed using ris3u [12] [10], one of the GRASP2K programs. Subsequently, this density is fitted to the polynomial function $b(r)$ so that the coefficients $b_{i,N}$ and their differences $\Delta b_{k,N}$ can be calculated. Finally, the level and frequency electronic factors, F_i and $F_{k,N}$, are deduced for the reference isotope A. This approach is not constrained to any approximated model describing the nuclear charge density distributions. Therefore, the realistic nuclear radial moments extracted from the Skyrme-type UDF1 interaction can be used in order to estimate the frequency shifts for several transitions and isotope pairs.

4.2.3 Validation of perturbative method

Since the variational approach stands so far for the best approximation to the field shifts, this method will serve as the verification instrument for the newly introduced perturbative method. The charge distributions in the VA are based on a two-parameter spherical Fermi model. For this model we adopt the same rms radii as given in Angelis & Marinova [2] that was used in the VA and for higher moments given by the Fermi model, should be virtually identical.

The validation of the RFS is illustrated in Figure 4.1, for three different Lithium-like lead isotope pairs and two different transitions k. In each pair, the ^{208}Pb is used as the reference isotope A and the electronic field shift factors are deduced for this nucleus. Hence, the frequency field shifts are plotted in relation to the mass number A' of the non-reference isotope. As seen in Figure 4.1, after adding all four expansion terms (red circle), the frequency field shifts $\delta\nu_k^{(1)208,A'}$ almost perfectly agree with the $\delta\nu_{k,VA}^{208,A'}$ (black square) resulting from the variational approach described in 4.2.1. Namely, the perturbative method provides us with rather satisfactory results. Additionally, the accumulated frequency field shift values, $\delta\nu_{k,\sum_{N=1,n}}^{208,A'}$ for $n = 1, 2, 3$, are displayed in the same plot for all three isotope pair combinations $208, A'$. The $\delta\nu_{k,\sum_{N=1,n}}^{208,A'}$ give three different frequency field shift values after each expansion term has been consecutively added, before the final $\delta\nu_k^{(1)208,A'}$ is deduced. We notice that for $n = 1$, we obtain $\delta\nu_{k,\sum_{N=1,1}}^{208,A'} = F_{k,1}\delta\left\langle r^2\right\rangle^{208,A'}$(green ring), which is the frequency field shift estimated using the assumption of constant electron density inside the nucleus. It is noteworthy here that the higher than second order moments evidently play an important role in the expansion of the reformulated frequency field shift, proving that the shape of the electron density inside such heavy nuclear systems always needs to be taken into account.

In order to perform a quantitative comparison of the contribution rate from each expansion term, the isolated term contributions are presented in Table 4 for the isotope pair ^{208,200}Pb. The accumulated contributions and contribution percentages are also displayed. As seen in Table 4, the terms that include the nuclear radial moments differences $\delta\left\langle r^{2N}\right\rangle^{208,200}$ for

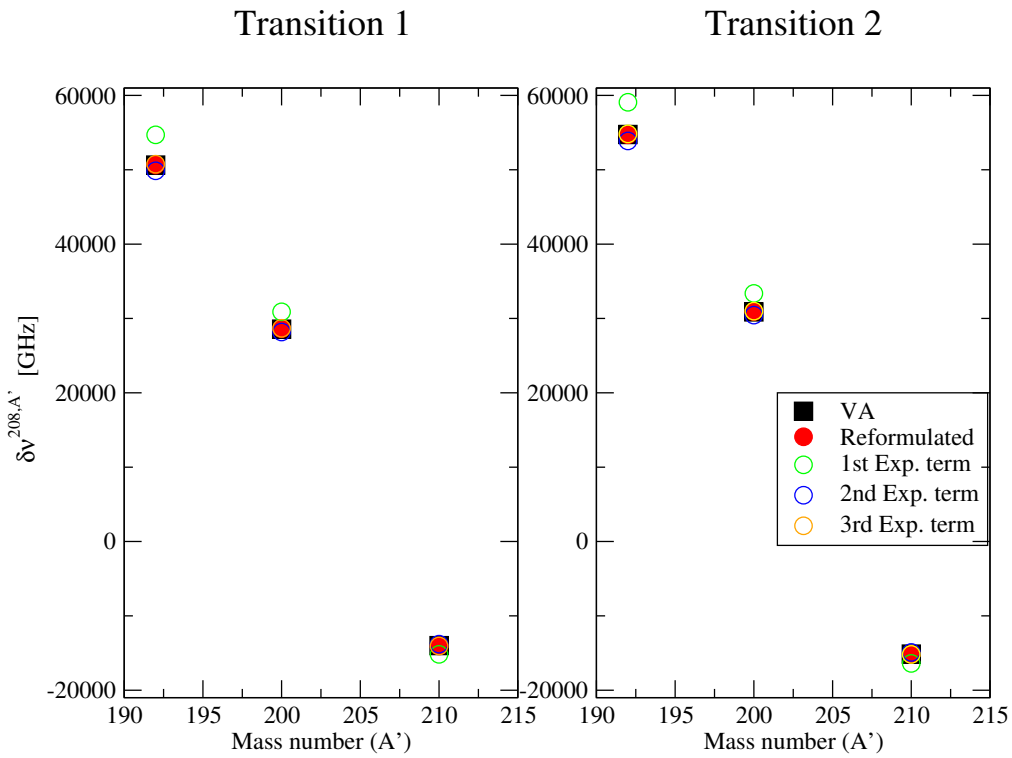

Figure 4.1: The frequency field shift $\delta\nu^{208,A'}$ for the Li-like Pb isotope pairs with $A' = 192, 200$ and 210. "Transition 1" refers to $1s^2 2s\ {}^2S_{1/2^+} \longrightarrow 1s^2 2p\ {}^2P_{1/2^-}$ transition, while "transition 2" is addressed to the $1s^2 2s\ {}^2S_{1/2^+} \longrightarrow 1s^2 2p\ {}^2P_{3/2^-}$ transition. The $\delta\nu_{VA}^{208,A'}$ resulting from the variational approach (VA) calculations, as well as the accumulated frequency field shifts $\delta\nu_{\sum_{N=1,n}}^{208,A'} = \sum_{N=1}^{n} F_{k,N}\delta\left\langle r^{2N}\right\rangle^{208,A'}$ for $n = 1, 2, 3, 4$ resulting from the perturbative approach, are separately demonstrated.

n	$\delta\nu_n^{208,200}$[GHz]	$\delta\nu_{\sum_{N=1,n}}^{208,200}$ [GHz]	$\frac{\delta\nu_{\sum_{N=1,n}}^{208,200}}{\delta\nu_{VA}^{208,200}}$[%]	$\frac{\delta\nu_n^{208,200}}{\delta\nu_{VA}^{208,200}}$[%]
1	30895.8235	30895.8235	108.172	108.172
2	-2717.8996	28177.9239	98.656	-9.516
3	505.9503	28683.8742	100.428	1.771
4	-59.2375	28624.6367	100.220	-0.207
$\delta\nu_{VA}^{208,200}$		28561.7494	100	

Table 4: Column two contains the isolated contributions $\delta\nu_n^{208,200} = F_{k,n}\delta\left\langle r^{2n}\right\rangle^{208,200}$ that each one out of the four in total expansion terms gives to the final $\sum_{N=1}^{4} F_{k,N}\delta\left\langle r^{2N}\right\rangle^{208,200}$ frequency field shift value of the ^{208,200}Pb pair calculated for $1s^2 2s\ ^2S_{1/2^+} \longrightarrow 1s^2 2p\ ^2P_{1/2^-}$ transition, whilst column three displays the accumulated contributions $\delta\nu_{\sum_{N=1,n}}^{208,200} = \sum_{N=1}^{n} F_{k,N}\delta\left\langle r^{2N}\right\rangle^{208,200}$. The $\left\langle r^2\right\rangle$ values are taken from Angelis & Marinova [2]. In column four, the matching percentage of the accumulated contributions is estimated based on the $\delta\nu_{VA}^{208,200}$ value. Lastly, the matching percentages of the isolated contributions are presented in column five.

$N = 2, 3, 4$ give almost 8% contribution to a precise evaluation of the field shifts, meaning that the constant electron density approximation is not good enough for the description of the heavy nuclear systems. Nonetheless, the major correction comes from the second expansion term that takes into account the differences between the r^4 moments. However, from the values of the accumulated percentages we draw the conclusion that the expansion converges to a slightly higher value than the one given by the $\delta\nu_{VA}^{208,200}$. Thus, the reformulation of the field shift remains an approximation to the "exact" VA method. The observed discrepancy is mainly due to the fact that the same electron density, deduced for the reference isotope $A = 208$, is used in both nuclei. Other assumptions that have been made throughout the formulation of the perturbative approach are expected to play a minor role.

5 The effect of realistic nuclear charge distributions

In chapter 4, the alternative approach introduced for estimating field shifts was validated. This approach is rather powerful since it enables the investigation of the effect that more realistic nuclear charge distributions have on level and frequency field shifts. In this section, we initially focus on the magnitude of the higher order contributions in the reformulated field shift, using theoretically predicted r^4, r^6 and r^8 moments. The corrections provided by the realistic charge distributions are compared to the uncertainties of the experimentally observed field shifts. Conclusions can then be drawn on the importance of such corrections depending on whether or not these could be detected by making use of the current experimental techniques. Ultimately, extraction of nuclear radial moment differences, $\delta\left\langle r^{2N}\right\rangle$ for $N = 1, 2, 3$ and 4, is discussed assuming that four independent transitions are available. However, a novel approach, where only two transitions are needed for the extraction of higher

order radial moments, will also be outlined.

5.1 Higher order moments in field shift

In the electronic calculations, the shape of the nuclear charge density distribution is approximated by the two-parameter spherical Fermi model described in subsection 3.2.2. However, the reformulation of the field shift enables calculations based on realistic nuclear charge distributions. Hence, the main objective in this section is to examine the magnitude of the corrections $\delta\nu_{realistic} - \delta\nu_{Fermi}$. We fit the Fermi distribution so that it has the same $\langle r^2 \rangle$ value as the realistic distribution. Then:

$$\delta\nu_{Fermi} = F_{k,1}\delta \left\langle r^2 \right\rangle_{realistic} + \sum_{N=2}^{4} F_{k,N}\delta \left\langle r^{2N} \right\rangle_{Fermi},$$

and

$$\delta\nu_{realistic} = \sum_{N=1}^{4} F_{k,N}\delta \left\langle r^{2N} \right\rangle_{realistic}.$$

Therefore, the frequency field shifts calculated using realistic charge distributions can be equivalently written:

$$\delta\nu_{realistic} = F_{k,1}\delta \left\langle r^2 \right\rangle_{realistic} + \sum_{N=2}^{4} F_{k,N}\delta \left\langle r^{2N} \right\rangle_{Fermi} + (\delta\nu_{realistic} - \delta\nu_{Fermi}),$$

treating the correction $\delta\nu_{realistic} - \delta\nu_{Fermi}$ as an additional term. For spherical nuclei, the realistic nuclear radial moments are extracted from the charge density distributions described by the Skyrme-based UDF1 interaction (see chapter 3). For deformed nuclei the realistic nuclear moments are calculated with the same interaction using the program HFBTHO (2.00d) [22].

We focus on heavy nuclear systems where the splitting of the energy values and transitions are larger. Besides, it is in these systems where the higher order moments contribute to a considerable extent. The orbitals that are affected the most by the change in the nuclear charge distributions between the isotopes are the ones closest to the nucleus. Therefore, transitions exclusively between s and p orbitals are examined here.

5.1.1 Spherical nuclei

The contribution from the "correction term" $\delta\nu_{realistic} - \delta\nu_{Fermi}$ is plotted in Figure 5.1 for a variety of Lithium-like systems with spherical nuclei. The Li-like system of lead Pb^{79+}, for which several isotope pair combinations have been studied, is of main interest. As seen in Figure 5.1, the absolute magnitude of the "correction term" mainly depends on the difference between the neutron number $\Delta N^{208,A'}$(or equivalently the difference between the mass number $\Delta A^{208,A'}$) for the isotopes $208, A'$ of the chosen pair. The larger the difference $\Delta N^{208,A'}$ is, the more important the role of the corrections becomes. When more neutrons are added it is expected that they will pull out the protons, leading to an increased diffuseness of the distribution. This effect is not included in the Fermi model and may be a reason for the

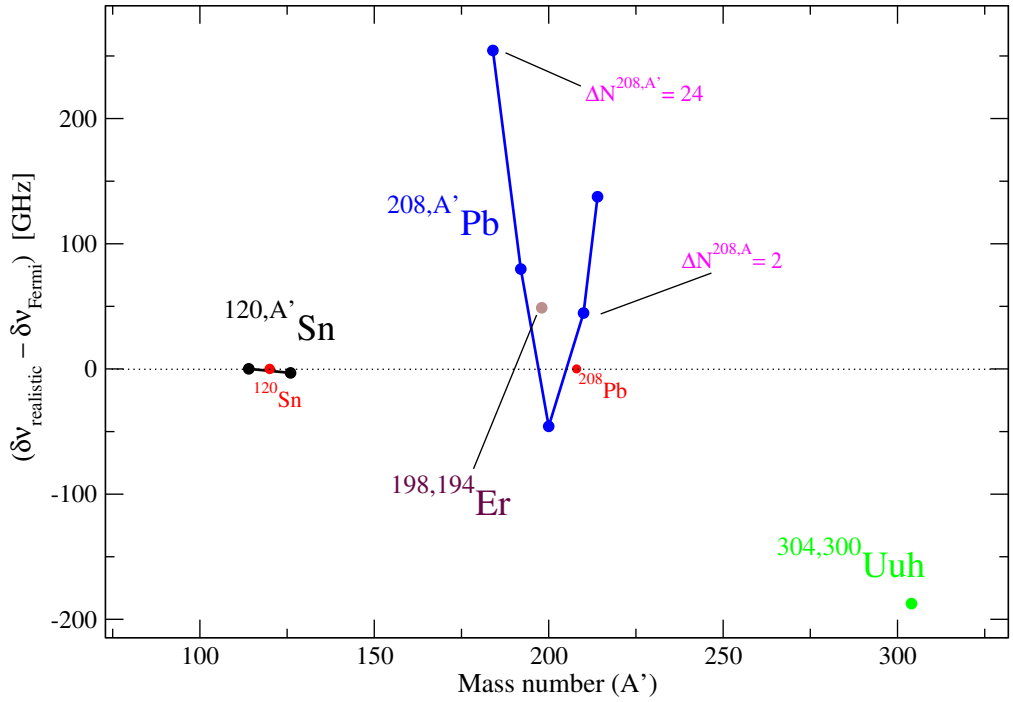

Figure 5.1: The corrections $\delta\nu_{realistic} - \delta\nu_{Fermi}$ to the frequency field shift calculations in relation to the mass number A' of the non-reference isotope. The results for the Li-like lead Pb^{79+} isotope pairs $^{208,A'}$Pb for $A' = 184, 192, 200, 210$ and 214 are illustrated in blue and the ones for the Li-like tin, ^{120,114}Sn and ^{120,126}Sn, in black. The reference isotopes used in these pair combinations, ^{208}Pb and ^{120}Sn, are pointed out with red. The result for the Li-like ununhexium pair ^{300,304}Uuh is shown in green. All plotted values refer to the transition $1s^2 2s\ ^2S_{1/2^+} \longrightarrow 1s^2 2p\ ^2P_{1/2^-}$.

n	$\delta\nu_n^{208,200}$[GHz]	$\delta\nu_{\sum_{N=1,n}}^{208,200}$[GHz]	$\frac{\delta\nu_{\sum_{N=1,n}}^{208,200}}{\delta\nu_{\sum_{N=1,5}}^{208,200}}$[%]	$\frac{\delta\nu_n^{208,200}}{\delta\nu_{\sum_{N=1,5}}^{208,200}}$[%]
1	35965.7809	35965.7809	108.205	108.205
2	-3210.1387	32755.6422	98.547	-9.658
3	599.4241	33355.0663	100.351	1.804
4	-70.7353	33284.3311	100.138	-0.203
5	-45.8809	33238.4501	100	-0.138

Table 5: Column two contains the isolated contributions $\delta\nu_n^{208,200}$ to the final frequency field shift value of the ^{208,200}Pb pair and the transition $1s^2 2s\ ^2S_{1/2^+} \longrightarrow 1s^2 2p\ ^2P_{1/2^-}$. For $n = 1, 2, 3$ and 4, $\delta\nu_n^{208,200} = F_{k,n}\delta\left\langle r^{2n}\right\rangle^{208,200}$ are given by the expansion terms of the reformulated frequency field shift. The $\delta\left\langle r^2\right\rangle$ is given by the realistic rms radii values of the isotopes, based on the UDF1 interaction, while $\delta\left\langle r^{2N}\right\rangle$ for $n = 2, 3, 4$ are given by the higher moments reproduced using a Fermi model that is formed on the UDF1 rms radii. Lastly, $\delta\nu_5^{208,200}$ represents the "correction term" $\delta\nu_{realistic} - \delta\nu_{Fermi}$. Column three displays the accumulated contributions $\delta\nu_{\sum_{N=1,n}}^{208,200}$, with $\delta\nu_{\sum_{N=1,5}}^{208,200}$ being the $\delta\nu_{realistic}$. In column four, the matching percentage of the accumulated contributions is estimated based on the final $\delta\nu_{realistic}$ value, whilst column five contains the matching percentages of the isolated contributions.

observed difference. However, these corrections are tiny for the much lighter system of (Li-like) Tin. In order to stress the larger magnitude of the effect that realistic higher order nuclear moments have on the frequency field shift estimated in heavy systems, the value of $\delta\nu_{realistic} - \delta\nu_{Fermi}$ has been calculated for the extreme case of the superheavy neutron-rich ununhexium element of proton number $Z = 116$. As seen in Figure 5.1, even for the small change $\Delta N = 4$, the corrections in superheavy systems can be hundred times larger than the ones in lighter systems.

A quantitative analysis of the magnitude of the "correction term" $\delta\nu_{realistic} - \delta\nu_{Fermi}$, as well as its contribution percentage to the final realistic frequency field shift value $\delta\nu_{realistic}$ for the isotope pair ^{208,200}Pb is displayed in Table 5. As seen in Table 5, the additional term $\delta\nu_{realistic} - \delta\nu_{Fermi}$ gives $\simeq 0.14\%$ contribution, which is smaller than the one resulting from the fourth expansion term. However, for isotope pairs with larger ΔN, like the ^{208,184}Pb, the correction adds a contribution that reaches 0.26%, which in this case is larger than the contribution of the last expansion term ($\simeq 0.2\%$). Therefore, we deduce that even in nuclear systems that are spherical the two-parameter Fermi model may not always provide a satisfactory description of the higher order moments that are used in the calculations of the RFS.

5.1.2 Deformed nuclei

The two-parameter Fermi model does not take into account the effect of deformation. As a result, the effect of the realistic charge distributions on the field shifts is expected to be even larger in atomic systems where the nuclei are deformed. In such systems, the axially symmetric deformed Fermi model is suggested to be used instead. The nuclear charge distributions are in this case given by:

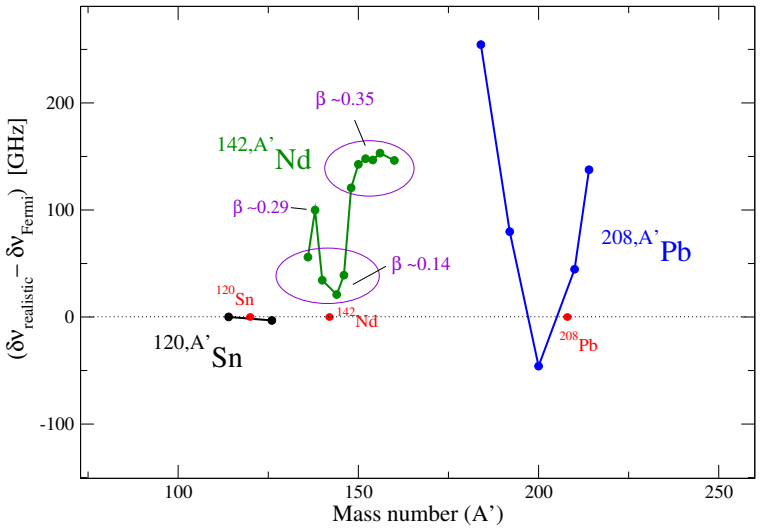

Figure 5.2: The corrections $\delta\nu_{realistic} - \delta\nu_{Fermi}$ to the frequency field shift calculations in relation to the mass number A' of the non-reference isotope. The results for the Li-like spherical lead Pb^{79+} isotope pairs are illustrated in blue, while Li-like deformed neodymium Nd^{57+} isotope pairs are displayed in green. For Nd^{57+}, the magnitude of the quadrupole deformation parameter β of the non-reference isotopes A' is indicatively shown for two different isotope groups. The reference isotopes used in the pair combinations, ^{208}Pb, ^{142}Nd and ^{120}Sn, are all spherical and are pointed out with red. All plotted values refer to the $1s^2 2s\ ^2S_{1/2^+} \longrightarrow 1s^2 2p\ ^2P_{1/2^-}$ transition.

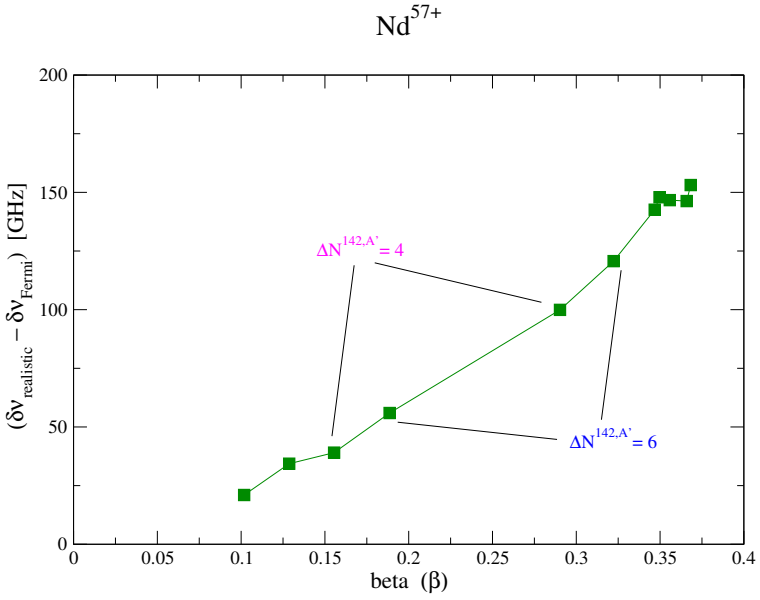

Figure 5.3: The corrections $\delta\nu_{realistic} - \delta\nu_{Fermi}$ to the frequency field shift calculations in relation to the quadrupole deformation parameter β of the non-reference A' isotope for various Nd^{57+} isotope pairs. In all pairs, the reference isotope is the spherical ^{142}Nd. Two cases of isotope pairs 142, A' with the same difference $\Delta N^{142,A'}$ in the neutron number but different $\delta\nu_{realistic} - \delta\nu_{Fermi}$ magnitude, due to the deformation β, are indicatively stressed.

$$\rho(r,\theta) = \frac{1}{1+e^{\frac{r-c(\theta)}{a}}},$$

where, if only quadrupole deformation is considered, $c(\theta) = c_0[1+\beta_{20}Y_{20}(\theta)]$. The "correction term" $\delta\nu_{realistic} - \delta\nu_{Fermi}$ can now be decomposed into two parts and written as:

$$\delta\nu_{realistic} - \delta\nu_{Fermi} = \left(\delta\nu_{realistic} - \delta\nu^{def}_{Fermi}\right) + \left(\delta\nu^{def}_{Fermi} - \delta\nu^{sph}_{Fermi}\right).$$

The $\delta\nu^{def}_{Fermi} - \delta\nu^{sph}_{Fermi}$ part isolates the magnitude of the effect of deformation, while the $\delta\nu_{realistic} - \delta\nu^{def}_{Fermi}$ part gives the magnitude of the corrections due to other effects, like for instance the density wiggles and the varied diffuseness that are not taken into account in the simplified Fermi approximation. In order to separately estimate the effect of deformation, we additionally calculated the frequency field shifts based on the higher order moments that are predicted by the deformed Fermi model. The deformed Fermi model is for each nuclear system developed based on a certain quadrupole deformation parameter β, in addition to the realistic rms radius of the nucleus, which is theoretically predicted by the HFBTHO (2.00d) program.

The Li-like system of neodymium is of great interest since the theoretically calculated frequency field shifts can be further compared to the available experimental data. Therefore, in Figure 5.2, the contribution to the frequency field shifts from the "correction term" $\delta\nu_{realistic} - \delta\nu_{Fermi}$ in relation to the mass number A' of the non-reference isotope is plotted for a variety of ion pairs Nd^{57+}, in addition to the Pb^{79+} and Sn^{47+} pairs plotted in Figure 5.1. While the reference isotope ^{142}Nd is spherical, the non-reference isotope is always deformed to a certain extent. As seen in Figure 5.2, the corrections become significant and comparable to the heavy Li-like system of lead whenever the value of the deformation parameter β for the non-reference isotope is large. On the other hand, in light systems and when the nuclei have approximately spherical shape the $\delta\nu_{realistic} - \delta\nu_{Fermi}$ value is negligible. This ascertainment has been already highlighted for the Li-like system of tin, where all isotopes in the pair combinations are purely spherical and as a consequence $\delta\nu_{realistic} - \delta\nu_{Fermi} \simeq 0$.

The magnitude of $\delta\nu_{realistic} - \delta\nu_{Fermi}$ in relation to the deformation parameter β of the non-reference isotope is plotted for the Nd^{57+} ion pairs in Figure 5.3. As seen in Figure 5.3, there is roughly a quadratic increase of the $\delta\nu_{realistic} - \delta\nu_{Fermi}$ value with the deformation. Therefore, in lighter and deformed nuclear systems, we deduce that the change in the neutron number $\Delta N^{A,A'}$ between two isotopes is not as an important factor for the estimation of the correction $\delta\nu_{realistic} - \delta\nu_{Fermi}$ as it is in the heavier systems.

In order to be able to draw conclusions about the significance of the "correction term" in comparison to the magnitude of each one of the expansion terms, as well as the total frequency field shift value $\delta\nu_{realistic}$, a quantitative analysis based on the isotope pair ^{142,150}Nd is displayed in Table 6. Table 6 provides a similar illustration of the contributions and the contribution percentages from each term as Table 5 does in 5.1.2. As seen in Table 6, the term $\delta\nu_{realistic} - \delta\nu_{Fermi}$ adds a contribution of $\simeq 1.16\%$ to the formulation of the frequency field shift $\delta\nu_{realistic}$. The contribution of the corrections provided by the usage of realistic nuclear data is now larger than the contribution from the third and fourth expansion terms when they are summed up, which reaches $\simeq 1.03\%$. More specifically, the major contribution comes from the $\delta\nu_5^{142,150}$ term, that is due to the usage of the deformed Fermi model. Further on, the $\delta\nu_6^{142,150}$ term, which is due to the wiggles, the skin diffuseness etc. of the realistic

n	$\delta\nu_n^{142,150}$[GHz]	$\delta\nu_{\sum_{N=1,n}}^{142,150}$[GHz]	$\frac{\delta\nu_{\sum_{N=1,n}}^{142,150}}{\delta\nu_{\sum_{N=1,6}}^{142,150}}$[%]	$\frac{\delta\nu_n^{142,150}}{\delta\nu_{\sum_{N=1,6}}^{142,150}}$[%]
1	-12979.2841	-12979.2841	105.609	105.609
2	647.7010	-12331.5831	100.339	-5.270
3	-113.5695	-12445.1526	101.263	0.924
4	12.6588	-12432.4937	101.160	-0.103
5	104.7742	-12327.7195	100.316	-0.844
6	37.8273	-12289.8922	100	-0.316

Table 6: In column two the isolated contributions $\delta\nu_n^{142,150}$ to the final frequency field shift value of the ^{142,150}Nd^{57+} pair calculated for $1s^2 2s\ ^2S_{1/2^+} \longrightarrow 1s^2 2p\ ^2P_{1/2^-}$ transition are shown. For $n = 1, 2, 3$ and 4, $\delta\nu_n^{142,150} = F_{k,n}\delta\left\langle r^{2n}\right\rangle^{142,150}$ are given by the expansion terms of the reformulated frequency field shift. The $\delta\left\langle r^2\right\rangle$ are given by the theoretically calculated rms radii of the isotopes, while $\delta\left\langle r^{2N}\right\rangle$ for $n = 2, 3, 4$ are given by the higher moments reproduced using the spherical two-parameter Fermi model that is formed on the theoretical rms radii. Lastly, the sum $\delta\nu_5^{142,150}+\delta\nu_6^{142,150}$ represents the correction $\delta\nu_{realistic}-\delta\nu_{Fermi}$, where $\delta\nu_5^{142,150} = \delta\nu_{Fermi}^{def}-\delta\nu_{Fermi}^{sph}$ and $\delta\nu_6^{142,150} = \delta\nu_{realistic}-\delta\nu_{Fermi}^{def}$. Column three displays the accumulated contributions $\delta\nu_{\sum_{N=1,n}}^{142,150}$, with $\delta\nu_{\sum_{N=1,6}}^{142,150}$ being the $\delta\nu_{realistic}$. In column four, the matching percentage of the accumulated contributions is estimated based on the final $\delta\nu_{realistic}$ value, whilst column five contains the matching percentages of the isolated contributions.

distributions, adds a contribution of $\simeq 0.32\%$ that, as seen in Table 6, exceeds the one from the fourth expansion term. Therefore, in deformed nuclear systems the two-parameter Fermi model seems to be even less appropriate for the description of the r^{2N}, $N = 2, 3$ and 4, moments than it was in the case of the spherical nuclei.

5.2 Experimental isotope shifts

The isotope shift (IS) calculations, and particularly the estimation of the corrections $\delta\nu_{realistic}-\delta\nu_{Fermi}$ to the field shifts that are provided when realistic nuclear data are used, become more meaningful when the comparison with experimental IS observations is feasible. The comparison of these corrections with the experimental uncertainties is also of interest since it will reveal if the corrections should be included in the analysis and eventually if they can be extracted from observed IS. In Li-like systems, highly accurate IS observations remain a challenge, since they are followed by relatively -compared to neutral systems- high uncertainties, both statistical and systematic. The Li-like system of neodymium Nd^{57+} has been studied and the observed isotope frequency shift is $\delta\nu_{IS,exp}^{142,150} = -9720(73)(145)$ GHz [(stat)(syst)] for the $1s^2 2s\ ^2S_{1/2^+} \longrightarrow 1s^2 2p\ ^2P_{1/2^-}$ transition and $\delta\nu_{IS,exp}^{142,150} = -10228(290)(484)$ GHz for the $1s^2 2s\ ^2S_{1/2^+} \longrightarrow 1s^2 2p\ ^2P_{3/2^-}$ transition [9]. The mass shift contribution is mainly significant in lighter systems. However, in order to obtain a reliable estimate of the "observed" frequency field shift, subtraction of the MS component is required. For the same transitions, the total mass shift, in the same work, were calculated to be $\delta\nu_{MS}^{142,150} = -387$ GHz and $\delta\nu_{MS}^{142,150} = -435$ GHz. Hence, the estimated "observed" field shift is finally $\delta\nu_{FS,exp}^{142,150} = -10107(73)(145)$ GHz

and $\delta\nu_{FS,exp}^{142,150} = -10663(290)(484)$ GHz, for each transition, respectively.

As seen in Table 6, for the $1s^22s\ ^2S_{1/2^+} \longrightarrow 1s^22p\ ^2P_{1/2^-}$ transition $\delta\nu_{Fermi}^{142,150} = -12432$ GHz, which after taking into account the corrections $\delta\nu_{realistic} - \delta\nu_{Fermi} = 142$ GHz takes the value $\delta\nu_{realistic}^{142,150} = -12290$ GHz. The calculated frequency field shift approaches the "observed" value after the "correction term" has been added, but $\delta\nu_{realistic}^{142,150}$ is still $\sim 20\%$ smaller than $\delta\nu_{FS,exp}^{142,150}$. A similar difference between "observed" and theoretically predicted frequency field shift is obtained for the $1s^22s\ ^2S_{1/2^+} \longrightarrow 1s^22p\ ^2P_{3/2^-}$ transition. Considering the differences between experimental and theoretical rms radii, the large difference between the corresponding frequency field shift values is not surprising. From the Angelis & Marinova compilation [2] we obtain $\delta\left\langle r^2\right\rangle_{exp}^{142,150} = 1.27$ fm^2, whereas the HFBTHO calculations result in $\delta\left\langle r^2\right\rangle_{realistic}^{142,150} = 1.64$ fm^2 ($\sim 20\%$ larger). The calculated charge distributions are not expected to be 100% exact when it comes to rms radii and particularly $\delta\left\langle r^2\right\rangle$ values. However, they should be realistic in terms of nuclear shapes and deformation and thus providing a more representative description of the higher order moments.

In the particular case of ^{142,150}Nd where the target isotope ^{150}Nd is deformed, the correction is $\delta\nu_{realistic} - \delta\nu_{Fermi} = 142$ GHz > 73 GHz, which is the magnitude of the statistical uncertainty in the measurement of the $\delta\nu_{IS,exp}^{142,150}$. The role of the "correction term" $\delta\nu_{realistic} - \delta\nu_{Fermi}$ is even more stressed when the higher moments differences $\delta\left\langle r^{2N}\right\rangle$ are extracted from the observed IS. Taking $\delta\nu_{FS,exp}^{142,150} = -10107(73)(145)$ GHz for the $1s^22s\ ^2S_{1/2^+} \longrightarrow 1s^22p\ ^2P_{1/2^-}$ transition, we can extract $\delta\left\langle r^2\right\rangle$ assuming a linear dependence:

$$\delta\nu_{FS,exp}^{142,150} \simeq C\delta\left\langle r^2\right\rangle.$$

The constant C for this particular transition is estimated using GRASP2K. We performed separate MCDHF calculations for ^{142}Nd ($\left\langle r^2\right\rangle^{1/2} = 4.9118$ fm^2) and ^{150}Nd ($\left\langle r^2\right\rangle^{1/2} = 5.0415$ fm^2), having as a reference the former isotope and using $t = 2.30$ fm for both isotopes. The reformulated field shift is $\delta\nu^{142,150} = -9745$ GHz and the "effective" field shift electronic factor becomes:

$$F = \frac{\delta\nu^{142,150}}{\delta\left\langle r^2\right\rangle^{142,150}} = \frac{-9745}{1.2909} = -7549\frac{\text{GHz}}{\text{fm}^2}.$$

Assuming a "dummy" isotope with $\left\langle r^2\right\rangle = \left\langle r^2\right\rangle^{142} + 1.00$ fm^2 and calculating the relative field shift yields an electronic factor F' that has almost the same magnitude as the one calculated before so that $F' \simeq F$. Therefore, we can, to a good enough approximation, assume that $F = C$ and rely on the linearity of the field shift parameter in GHz/fm^2. Using the "observed" field shift, we obtain:

$$\delta\left\langle r^2\right\rangle = \frac{\delta\nu_{FS,exp}^{142,150}}{F} = 1.3389\text{fm}^2.$$

By taking into account the effect of the realistic charge distribution, the field shift electronic factor takes the value:

$$F_{cor} = F + \frac{\delta\nu_{realistic} - \delta\nu_{Fermi}}{\delta\left\langle r^2\right\rangle_{realistic}} = -7462\frac{\text{GHz}}{\text{fm}^2}.$$

Using again the "observed" field shift, we obtain:

$$\delta\left\langle r^2\right\rangle_{cor} = \frac{\delta\nu_{FS,exp}^{142,150}}{F_{cor}} = 1.3545\text{fm}^2.$$

In the work by Brandau et al. [9], the extracted $\delta\langle r^2\rangle$ for the same transition is 1.36(1)(3) fm^2. The $\delta\langle r^2\rangle$ and $\delta\langle r^2\rangle_{cor}$ that we estimated above are slightly different due to the fact that some small corrections from additional effects have been neglected throughout our calculations of the "observed" field shift, whereas in the analysis of Brandau these effects have been taken into account and subtracted from the observed IS $\delta\nu_{IS,exp}^{142,150}$. The difference between the $\delta\langle r^2\rangle$ and the $\delta\langle r^2\rangle_{cor}$ is ~ 0.016 fm^2, which is larger than the statistical error but smaller than the systematical error. Hence, in this case the effect from the realistic charge distributions is important and comparable in magnitude to the observed uncertainty. It is possible to double-check the $\delta\langle r^2\rangle$ value by using the observed IS of the second available transition and calculating the relevant electronic factor F, but for this transition both statistical and systematic error are larger and thus better resolution is needed in order to see the effect of the realistic charge distributions.

5.3 Extracting higher moments from data

The reformulation of the field shift combined with experimental isotope shifts $\delta\nu_{k,IS}^{(exp)A,A'}$ enables the extraction of the radial nuclear moments r^{2N}, $N = 1, 2, 3, 4$ for the target isotope A', when the corresponding moments are known for the reference isotope A. Thus, conclusions can be drawn about the nuclear shapes, deformations, density wiggles and other nuclear properties. The extraction of all four radial moments requires four independent transitions k to be available. A system of four equations is then solved for:

$$\delta\nu_{k,IS}^{exp} - \delta\nu_{k,MS} = F_{k,1}\delta\left\langle r^2\right\rangle + F_{k,2}\delta\left\langle r^4\right\rangle + F_{k,3}\delta\left\langle r^6\right\rangle + F_{k,4}\delta\left\langle r^8\right\rangle,$$

where $k = 1, 2, 3, 4$. The frequency electronic factors $F_{k,N}$ and the frequency mass shift parameters $\Delta K_{k,MS}$, different for each transition k, may theoretically be calculated using an atomic structure code such as GRASP2K. However, it is rare that observed IS are available for four transitions and in addition such systems of equations cannot be formed so that they give trustworthy solutions for the higher than second order moments.

Looking back at Figure 4.1, we can say that the major correction, to the approximation that assumes constant electron density $\rho_i^e(\vec{r}) = \rho_i^e(0)$, comes from the second expansion term, i.e. $F_{k,2}\delta\langle r^4\rangle$, which takes into account the differences between the r^4 moments. Nonetheless, the contribution from the $\sum_{N=3}^{4} F_{k,N}\delta\left\langle r^{2N}\right\rangle$ part of the expression for the reformulated frequency field shift remains not negligible. This is also illustrated in Figure 5.4, where the matching percentage to the final frequency shift value $\sum_{N=1}^{4} F_{k,N}\delta\left\langle r^{2N}\right\rangle^{208,200}$ of the isotope pair ^{208,200}Pb has been plotted after each term is added. Obviously, when the fourth expansion term is taken into account, the final field shift value is reached. As seen in Figure 5.4, the $4th$ order radial moments add $\sim 10\%$ contribution, the $6th$ moments add $\sim 2\%$ contribution and the last term, which contains the $8th$ order moments, contributes with much less. However, a re-arrangement of the sum that gives the RFS could possibly lead to faster convergence.

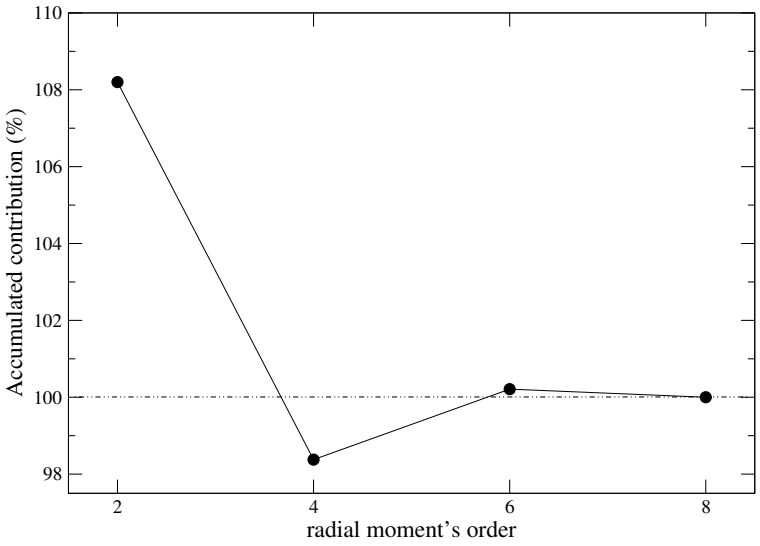

Figure 5.4: The matching percentage of the accumulated contributions $\delta\nu^{208,200}_{\sum_{N=1,n}}$, $n = 1, 2, 3, 4$, to the final frequency shift value $\delta\nu^{208,200} = \delta\nu^{208,200}_{\sum_{N=1,4}} = \sum_{N=1}^{4} F_{k,N}\delta\left\langle r^{2N}\right\rangle^{208,200}$, for the ^{208,200}Pb pair and the $1s^2 2s\ ^2S_{1/2^+} \longrightarrow 1s^2 2p\ ^2P_{1/2^-}$ transition.

5.3.1 RFS expansion in orthonormal basis

The RFS is, for a certain transition, given by the expansion:

$$\sum_{N=1}^{4} F_N \delta\left\langle r^{2N}\right\rangle = F_1\delta\left\langle r^2\right\rangle + F_2\delta\left\langle r^4\right\rangle + F_3\delta\left\langle r^6\right\rangle + F_4\delta\left\langle r^8\right\rangle,$$

where the field shift electronic factors F_N play the role of the expansion coefficients. However, the set of r^{2N} forms a basis $\{r^2, r^4, r^6, r^8\}$ that is not orthonormal. One can orthonormalize this basis into some orthogonal functions y_N by using the Gram-Schmidt method. Here, we orthonormalize the initial basis with respect to the scalar product:

$$\langle u \mid v\rangle = \int u * v * w r^2 dr,$$

where w is the weight function that approximates the nucleus. Since the functions y_N, forming the basis $\{y_1, y_2, y_3, y_4\}$, will probe different aspects of the nuclear charge distribution within the nuclear volume, we expect that the new expansion:

$$\sum_{N=1}^{4} c_N \delta\left\langle y_N\right\rangle = c_1\delta\left\langle y_1\right\rangle + c_2\delta\left\langle y_2\right\rangle + c_3\delta\left\langle y_3\right\rangle + c_4\delta\left\langle y_4\right\rangle,$$

will converge faster than $\sum_{N=1}^{4} F_N\delta\left\langle r^{2N}\right\rangle$. In the expression above, the c_N are the new expansion coefficients. Assuming that the nucleus can be approximated as a hard sphere, one can

use $w = \rho_0\Theta(R-r)$ with $R = 1.25A^{1/3}$. The value of ρ_0 is determined by the normalization condition: $4\pi\int\rho_0 r^2 dr = 1$. Following the Gram-Schmidt process, we obtain:

$$y_1 = \frac{3.46556}{\bar{A}^{2/3}}r^2$$

$$y_2 = -\frac{15.2051}{\bar{A}^{2/3}}r^2 + \frac{12.5116}{\bar{A}^{4/3}}r^4$$

$$y_3 = \frac{39.9503}{\bar{A}^{2/3}}r^2 - \frac{80.3573}{\bar{A}^{4/3}}r^4 + \frac{37.1429}{\bar{A}^{2}}r^6$$

$$y_4 = -\frac{82.4315}{\bar{A}^{2/3}}r^2 + \frac{293.927}{\bar{A}^{4/3}}r^4 - \frac{313.522}{\bar{A}^{2}}r^6 + \frac{103.367}{\bar{A}^{8/3}}r^8,$$

where $\bar{A}$ is taken as the average of the mass numbers of the two isotopes. The sum of the expansion terms has been re-arranged but $\sum_{N=1}^{4} F_N\delta\left\langle r^{2N}\right\rangle = \sum_{N=1}^{4} c_N\delta\left\langle y_N\right\rangle$ must still hold. The c_N coefficients can be found e.g. through equating same order terms in the above equation. Hence, the new coefficients are:

$$c_1 = 0.288554\bar{A}^{2/3}F_1 + 0.350673\bar{A}^{4/3}F_1 + 0.448303\bar{A}^{2}F_3 + 0.592709\bar{A}^{8/3}F_4$$

$$c_2 = 0.0799258\bar{A}^{4/3}F_2 + 0.172916\bar{A}^{2}F_3 + 0.2972\bar{A}^{8/3}F_4$$

$$c_3 = 0.026923\bar{A}^{2}F_3 + 0.08166\bar{A}^{8/3}F_4$$

$$c_4 = 0.00967424\bar{A}^{8/3}F_4$$

Now, the RFS is given by the new summation $\sum_{N=1}^{4} c_N\delta\left\langle y_N\right\rangle$ and the matching percentage to the final field shift after each term has been added differs from the one when the original summation is used. As seen in Figure 5.5, the orthogonal expansion converges substantially faster than before. By taking into account only the first term, the frequency field shift is already much closer to the final value. The $4th$ order radial moments add $\sim 3.5\%$ contribution, the $6th$ moments add $\sim 0.18\%$ contribution, while the $8th$ moments add a contribution of $\sim 0.016\%$. The contribution from the third expansion term that contains the $6th$ moments $0.18\% < 0.21\%$, which is the contribution of the last term in the original summation. In fact, only $\delta\left\langle r^2\right\rangle$ and $\delta\left\langle r^4\right\rangle$ play a role if the sum is re-arranged.

5.3.2 Extraction of $\delta\left\langle r^2\right\rangle$ and $\delta\left\langle r^4\right\rangle$

The RFS for a pair of isotopes A, A' and a transition k can, as has been showed above, to a very good approximation be expressed as:

$$\delta\nu_{k,FS}^{A,A'} = c_{k,1}\delta\left\langle y_1\right\rangle + c_{k,2}\delta\left\langle y_2\right\rangle.$$

In case the IS is known for two transitions, a system of two equations can be formed. The $c_{k,1}$ and $c_{k,2}$ constants may be evaluated using the expressions displayed above. They depend on the electronic factors $F_{k,N}$ that are different for each transition and which are calculated

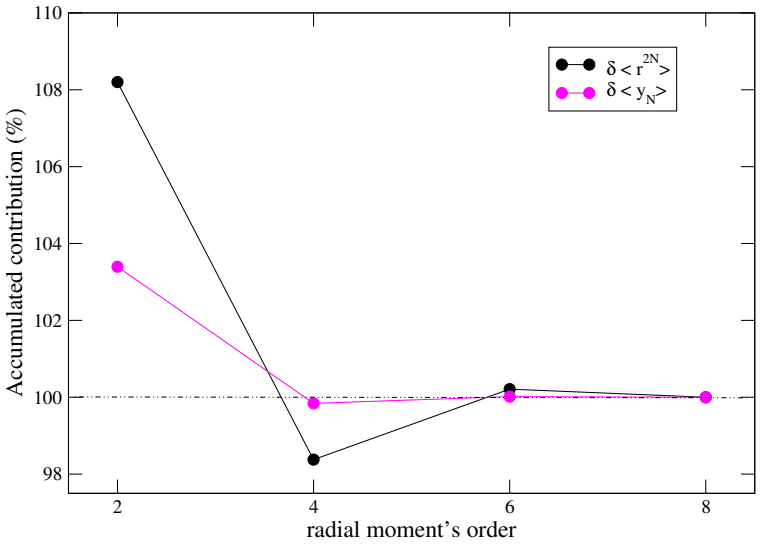

Figure 5.5: The matching percentage of the accumulated contributions $\delta\nu^{208,200}_{\sum_{N=1,n}}$, $n = 1,2,3,4$, to the final frequency shift value $\delta\nu^{208,200}_{\sum_{N=1,4}}$, is shown in black when the original summation $\sum_{N=1}^{4} F_N \delta \langle r^{2N} \rangle$ is used and in magenta when $\sum_{N=1}^{4} c_N \langle y_N \rangle$ is used. The plot refers again to the ^{208,200}Pb pair and $1s^2 2s\ ^2S_{1/2^+} \longrightarrow 1s^2 2p\ ^2P_{1/2^-}$ transition.

for the reference isotope A. Therefore, for two transitions, the problem takes the form of a matrix equation:

$$\begin{bmatrix} \delta\nu^{A,A'}_{1,FS} \\ \delta\nu^{A,A'}_{2,FS} \end{bmatrix} = \begin{bmatrix} c_{1,1} & c_{1,2} \\ c_{2,1} & c_{2,2} \end{bmatrix} \begin{bmatrix} \delta \langle y_1 \rangle \\ \delta \langle y_2 \rangle \end{bmatrix}.$$

The unknown y_1 and y_2 can thus be solved according to:

$$\begin{bmatrix} \delta \langle y_1 \rangle \\ \delta \langle y_2 \rangle \end{bmatrix} = C^{-1} \begin{bmatrix} \delta\nu^{A,A'}_{1,FS} \\ \delta\nu^{A,A'}_{2,FS} \end{bmatrix},$$

where C^{-1} is the inverse matrix of $\begin{bmatrix} c_{1,1} & c_{1,2} \\ c_{2,1} & c_{2,2} \end{bmatrix}$. The $\delta \langle r^2 \rangle$ and $\delta \langle r^4 \rangle$ are finally extracted by solving:

$$\begin{bmatrix} \delta \langle y_1 \rangle \\ \delta \langle y_2 \rangle \end{bmatrix} = \begin{bmatrix} 3.46556/\bar{A}^{2/3} & 0 \\ -15.2051/\bar{A}^{2/3} & 12.5116/\bar{A}^{4/3} \end{bmatrix} \begin{bmatrix} \delta \langle r^2 \rangle \\ \delta \langle r^4 \rangle \end{bmatrix}$$

In order to test the newly introduced "y-method" theoretical frequency field shifts were obtained by using the HFB nuclear radial moments. These frequency field shifts refer to the transitions $1s^2 2s\ ^2S_{1/2^+} \longrightarrow 1s^2 2p\ ^2P_{1/2^-}$ and $1s^2 2s\ ^2S_{1/2^+} \longrightarrow 1s^2 2p\ ^2P_{3/2^-}$, for the same -previously studied- isotope pairs of lead and neodymium. Using the calculated field shifts as pseudo-data, the $\delta \langle r^2 \rangle$ and $\delta \langle r^4 \rangle$ values can be deduced from the $\delta \langle y_1 \rangle$ and $\delta \langle y_2 \rangle$. In all cases, the extracted $\delta \langle r^2 \rangle$ are almost identical to the exact $\delta \langle r^2 \rangle_{HFB}$. The difference is less than 0.0002 fm^2 for all lead isotopes and the neodymium isotopes that are close to spherical. For the highly deformed neodymium isotopes, the difference is slightly larger, of the order

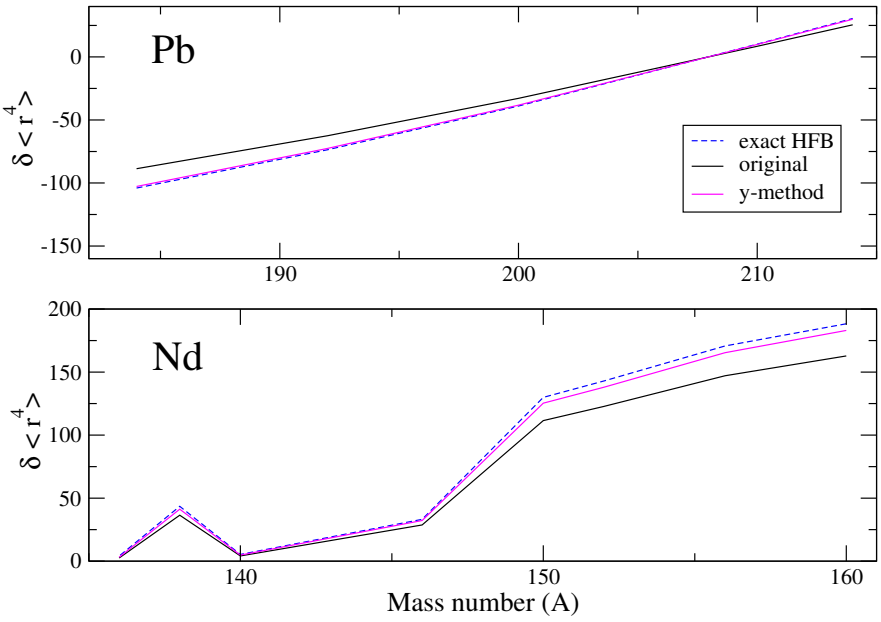

Figure 5.6: The extracted $\delta\langle r^4\rangle$ values for the lead (up) and neodymium (down) isotope pairs, previously studied. The blue dashed line represents the exact $\delta\langle r^4\rangle_{HFB}$ values, yielded from the HFB and HFBTHO calculations for the spherical lead and the deformed neodymium isotopes, respectively. The magenta line represents the $\delta\langle r^4\rangle$ extracted when $\delta\nu_{k,FS} = c_{k,1}\delta\langle y_1\rangle + c_{k,2}\delta\langle y_2\rangle$ is assumed, while the black line corresponds to the $\delta\langle r^4\rangle_{original}$ extracted when the original summation in $\delta\nu_{k,FS}$ has been used.

of $\simeq 0.0013$ fm^2, but still this represents a small discrepancy. In Figure 5.6, the extracted $\delta\langle r^4\rangle$ values have been plotted and compared to the exact $\delta\langle r^4\rangle_{HFB}$ values. In addition, the extracted $\delta\langle r^4\rangle_{orig}$ values using the original summation $\delta\nu_{k,FS}^{A,A'} = \sum_{N=1}^{4} F_{k,N}\delta\langle r^{2N}\rangle_{orig}$ for the expression of the RFS are illustrated in the same figure. In the latter case, in order to extract the $\delta\langle r^2\rangle_{orig}$ and $\delta\langle r^4\rangle_{orig}$ from two available transitions, we evidently take into account only the first two expansion terms assuming the approximate relation: $\delta\nu_{k,FS}^{A,A'} = F_{k,1}\delta\langle r^2\rangle_{orig} + F_{k,2}\delta\langle r^4\rangle_{orig}$. The matrix equation is then given by:

$$\begin{bmatrix} \delta\nu_{1,FS}^{A,A'} \\ \delta\nu_{2,FS}^{A,A'} \end{bmatrix} = \begin{bmatrix} F_{1,1} & F_{1,2} \\ F_{2,1} & F_{2,2} \end{bmatrix} \begin{bmatrix} \delta\langle r^2\rangle_{orig} \\ \delta\langle r^4\rangle_{orig} \end{bmatrix}.$$

As seen in Figure 5.6, when the re-arranged summation is used the extracted $\delta\langle r^4\rangle$ are in good agreement with the exact $\delta\langle r^4\rangle_{HFB}$, whereas the $\delta\langle r^4\rangle_{orig}$ display an observable discrepancy from them. The discrepancy between $\delta\langle r^4\rangle_{orig}$ and $\delta\langle r^4\rangle_{HFB}$ becomes significant, in the lead cases, when $\Delta N^{A,A'}$ is large and, in neodymium, when the non-reference isotope is deformed. Moreover, we note that $\delta\langle r^2\rangle_{orig}$ and $\delta\langle r^2\rangle_{HFB}$ do not display the same (almost) perfect match that $\delta\langle r^2\rangle$ and $\delta\langle r^2\rangle_{HFB}$ do. All in all, the new expression using the re-arranged summation for the RFS enables the determination of the differences between r^2 and r^4 moments, much more accurately than the original expression.

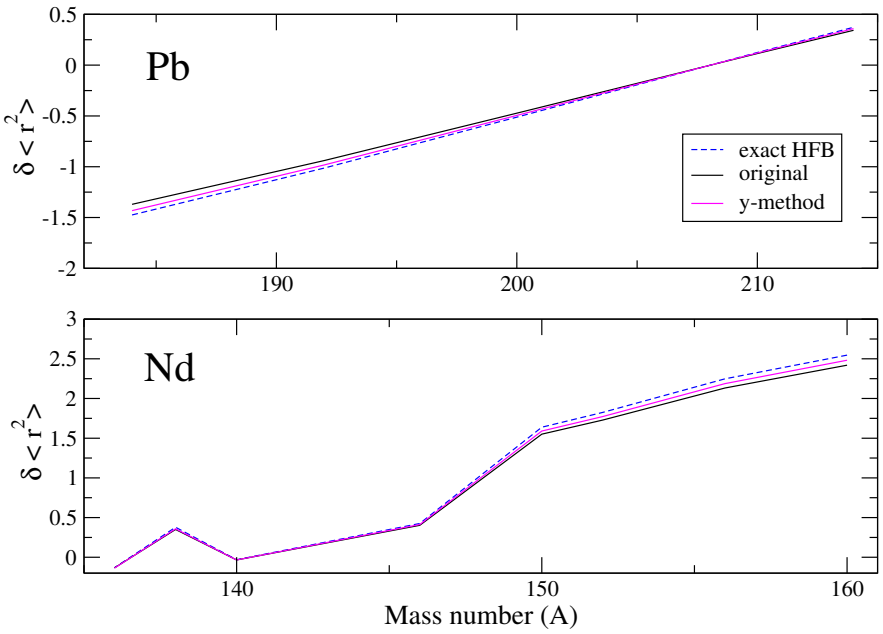

Figure 5.7: The extracted $\delta\langle r^2\rangle$ values for the lead (up) and neodymium (down) isotope pairs. The blue dashed line represents the exact $\delta\langle r^2\rangle_{HFB}$ values, the magenta line the $\delta\langle r^2\rangle$ extracted when $\delta\nu_{k,FS} = c_{k,1}y_1$ and the black line corresponds to the $\delta\langle r^2\rangle_{orig}$ extracted when $\delta\nu_{k,FS} = F_{k,1}\delta\langle r^2\rangle$.

Assuming now that we only want to extract $\delta\langle r^2\rangle$, we take $y_2 = 0$ so that the frequency field shift is roughly given by:

$$\delta\nu_{k,FS}^{A,A'} = c_{k,1}\delta\langle y_1\rangle .$$

For two available transitions as before, the matrix equation to be solved takes the form:

$$\begin{bmatrix} \delta\nu_{1,FS}^{A,A'} \\ \delta\nu_{2,FS}^{A,A'} \end{bmatrix} = \begin{bmatrix} c_{1,1} \\ c_{2,1} \end{bmatrix} (\delta\langle y_1\rangle) .$$

Solving for the unknown y_1:

$$\delta\langle y_1\rangle = \widetilde{C}^{-1} \begin{bmatrix} \delta\nu_{1,FS}^{A,A'} \\ \delta\nu_{2,FS}^{A,A'} \end{bmatrix},$$

where $\widetilde{C}^{-1}$ is the pseudo-inverse matrix of $\begin{bmatrix} c_{1,1} \\ c_{2,1} \end{bmatrix}$. Since C is not a square matrix, its inverse matrix C^{-1} cannot be determined. However, it is possible to construct its pseudo-inverse $\widetilde{C}^{-1}$. $\delta\langle r^2\rangle$ is finally extracted by solving:

$$\delta\langle y_1\rangle = \frac{3.46556}{A^{2/3}}\delta\langle r^2\rangle .$$

In Figure 5.7, the extracted $\delta\langle r^2\rangle$ have been plotted and compared to the exact $\delta\langle r^2\rangle_{HFB}$. The extracted $\delta\langle r^2\rangle_{orig}$ from the original summation have also been plotted in the same figure. For the extraction of $\delta\langle r^2\rangle_{orig}$, it has been assumed that $\delta\nu_{k,FS}^{A,A'} = F_{k,1}\delta\langle r^2\rangle$, i.e. the constant

density approximation. As seen in Figure 5.7, although the $\delta\langle r^2\rangle$ that correspond to the re-arranged summation are close enough to the $\delta\langle r^2\rangle_{HFB}$, they do not any more reproduce as well as before the exact values. Considering the fact that only the first expansion term is now taken into account when the matrix equation is solved, so that the RFS is roughly approximated, this observed discrepancy is expected. Indicatively, the displayed difference is now $\simeq 0.04$ fm^2 for the lead isotopes, less than 0.01 fm^2 for the spherical neodymium isotopes and between 0.06 and 0.04 fm^2 for the deformed ones. However, the re-arranged expression of the RFS keeps giving satisfactory enough results for the $\delta\langle r^2\rangle$ values. Furthermore, we note that the discrepancy between $\delta\langle r^2\rangle_{orig}$ and $\delta\langle r^2\rangle_{HFB}$ is again larger than the one obtained using the y-method. Thus, we deduce that the original RFS expression is not as appropriate as the new summation is, for either extracting both $\delta\langle r^2\rangle$ and $\delta\langle r^4\rangle$ or when extracting only the $\delta\langle r^2\rangle$.

5.3.3 Uncertainties in the extraction of $\delta\langle r^2\rangle$ and $\delta\langle r^4\rangle$

The $\delta\langle r^2\rangle$ and $\delta\langle r^4\rangle$ are extracted by solving the matrix equation:

$$\begin{bmatrix} \delta\nu_{1,FS}^{A,A'} \\ \delta\nu_{2,FS}^{A,A'} \end{bmatrix} = \begin{bmatrix} c_{1,1} & c_{1,2} \\ c_{2,1} & c_{2,2} \end{bmatrix} \begin{bmatrix} \delta\langle y_1\rangle \\ \delta\langle y_2\rangle \end{bmatrix}.$$

In order to be able to solve for y_1 and y_2, the matrix C must be invertible. If the matrix determinant is zero, then the matrix is singular and cannot be inverted. It is not rare that the determinant of such matrix can be really close to zero, but still non-zero. In this case, the matrix is close to singular and as a result the values of $\delta\langle y_1\rangle$ and $\delta\langle y_2\rangle$ will be hugely affected, even by a small change in the field shifts $\delta\nu_{1,FS}^{A,A'}$ and $\delta\nu_{2,FS}^{A,A'}$. Namely, the extracted $\delta\langle y_1\rangle$ and $\delta\langle y_2\rangle$, and as a consequence $\delta\langle r^2\rangle$ and $\delta\langle r^4\rangle$, will to a great degree be affected by the uncertainties in the observed IS, making the extraction of the radial nuclear moments with high accuracy not an easy task. A determinant equal to zero is obtained for the C matrix if the two equations are linearly dependent. In such case it is not possible to extract two unknowns. Therefore, the transitions considered should be as independent as possible.

As discussed before, when two RFS expansion terms are taken into consideration the extracted $\delta\langle r^2\rangle$ are virtually identical to $\delta\langle r^2\rangle_{HFB}$. On the other hand, when only the first RFS expansion term is considered the extracted $\delta\langle r^2\rangle$ are not as exact as before. However, in the latter case the uncertainties in the extraction of these values are minor due to the fact that the matrix equation has the form:

$$\begin{bmatrix} \delta\nu_{1,FS}^{A,A'} \\ \delta\nu_{2,FS}^{A,A'} \end{bmatrix} = \begin{bmatrix} c_{1,1} \\ c_{2,1} \end{bmatrix} (\delta\langle y_1\rangle)$$

and evidently, two equations are solved for just one unknown, that is the y_1. Therefore, the y_1 will be determined with much higher accuracy.

The extraction of $\delta\langle r^2\rangle$ and $\delta\langle r^4\rangle$ in subsection 5.3.2 was performed using theoretical $\delta\nu_{k,FS}$ values that are accurate to high precision (at least 10 digits). One may however assume an inaccuracy in the $\delta\nu_{k,FS}$ values and check the maximum change in the results when $\pm\epsilon$ is added to $\delta\nu_{k,FS}$. For example, choosing an ϵ corresponding to three correct digits, the equations can be solved for the two unknowns $\delta\langle y_1\rangle$ and $\delta\langle y_2\rangle$, but the resulting

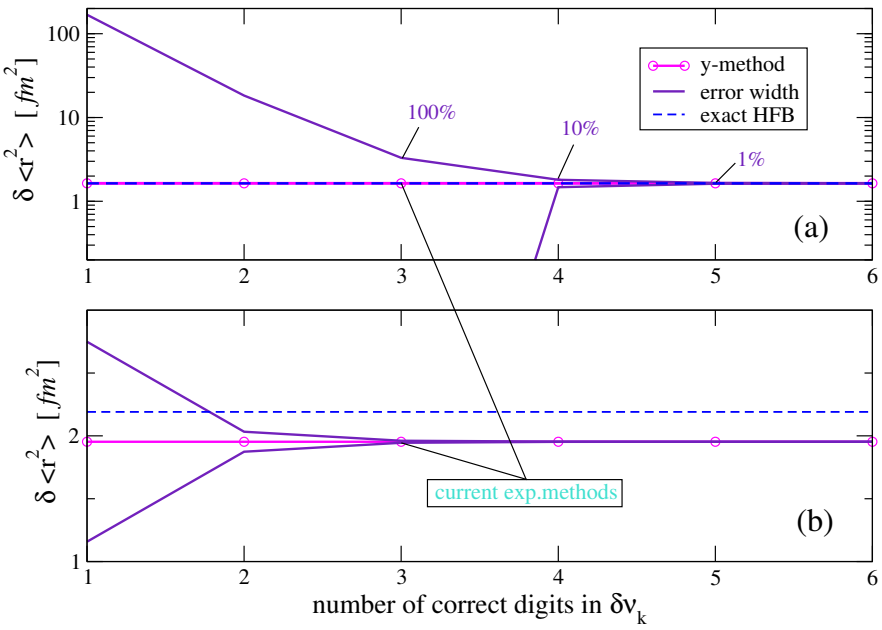

Figure 5.8: The uncertainty magnitude in the extraction of the $\delta\langle r^2\rangle^{142,150}$ (magenta line) in relation to the number of correct digits in $\delta\nu_k^{142,150}$, when two (a) and when only one (b) expansion term have been considered. The dashed blue line illustrates the exact $\delta\langle r^2\rangle_{HFB}$ value. The number of correct digits in the $\delta\nu_k^{142,150}$ measurement using the current experimental methods is pointed out.

uncertainties are rather large. For the lead isotopes, the error in $\delta\langle r^2\rangle$ is as large as half of the magnitude of the $\delta\langle r^2\rangle$ value, while for neodymium the error is even slightly larger than the $\delta\langle r^2\rangle$ value. On the contrary, when y_1 is the only unknown, the uncertainties are less than ± 0.0014 fm^2 and ± 0.0025 fm^2 for lead and neodymium, respectively. We note here that for neodymium the larger uncertainties are due to deformation. If the non-reference neodymium isotope is also spherical, then the uncertainty to the extraction of the $\delta\langle r^2\rangle$ is less than ± 0.0004.

In Figures 5.8 (a) and 5.9 , the magnitude of the uncertainty in the extraction of $\delta\langle r^2\rangle^{142,150}$ and $\delta\langle r^4\rangle^{142,150}$ is indicatively illustrated for different number of correct digits in the $\delta\nu_k^{142,150}$. As mentioned before, the results are rather sensitive to the number of correct digits that are available and as a consequence the scale of the error increases dramatically. For that reason, the logarithm of the uncertainties had to be plotted and this explains the behavior of the curve whenever the $\delta\langle r^2\rangle^{142,150}$ and $\delta\langle r^4\rangle^{142,150}$ take negative values. However, the magnitude of the errors is obvious from their positive maximum. As seen in Figure 5.8 (a), three correct digits result in a rather large uncertainty in the determination of $\delta\langle r^2\rangle^{142,150}$, when $\delta\langle r^4\rangle^{142,150}$ is determined at the same time. As seen in Figure 5.9, the same holds for the extracted $\delta\langle r^4\rangle^{142,150}$, which is determined with even greater uncertainty. Therefore, one can deduce that at least five correct digits are needed in order for $\delta\langle r^2\rangle^{142,150}$ and $\delta\langle r^4\rangle^{142,150}$ to be accurately calculated.

As seen in Figure 5.8 (b) in case we are willing to calculate only the $\delta\langle r^2\rangle^{142,150}$, three correct digits in $\delta\nu_k^{142,150}$ provide us with highly accurate results. Provided the current ex-

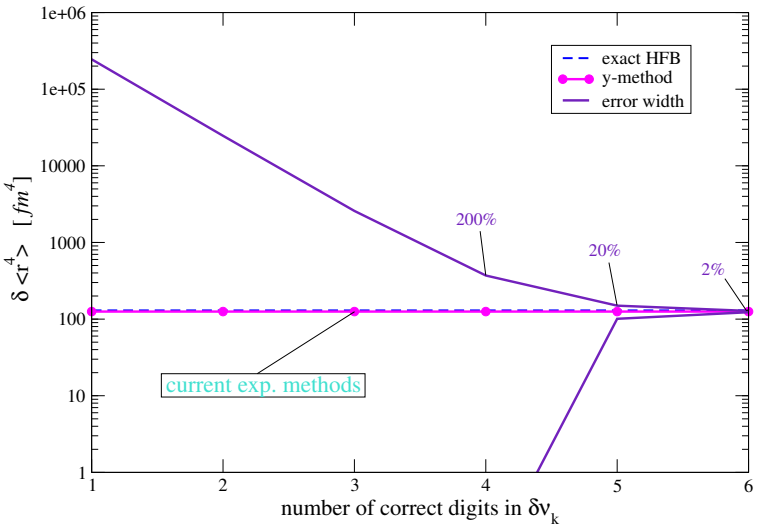

Figure 5.9: The uncertainty magnitude in the extraction of $\delta\langle r^4\rangle$ in relation to the number of correct digits in $\delta\nu_k^{142,150}$. The dashed blue line illustrates the exact $\delta\langle r^2\rangle_{HFB}$ value. The number of correct digits in the $\delta\nu_k^{142,150}$ measurement using the current experimental methods is pointed out.

perimental methods, the extraction of $\delta\langle r^2\rangle^{142,150}$ as the exclusive unknown may already be performed with high precision in the sense that the experimental errors do not influence the extracted $\delta\langle r^2\rangle^{142,150}$ values. However, the extracted $\delta\langle r^2\rangle^{142,150}$ still suffer from model errors depending on our assumptions made for $\delta\langle r^4\rangle^{142,150}$, and as a result they differ from the exact value (compare red with blue dashed line in Fig.5.8 (b)).

6 Results

The charge distributions resulting from different isotopes effect the electronic orbitals. Therefore, analogue atomic spectral lines from these isotopes display a small shift in energy, the so-called frequency isotope shift. Many of the atomic structure packages that are currently available for computing atomic properties approximate the nuclear charge distributions using the Fermi model. However, it seems that the observed isotope shift is rather sensitive to the nuclear properties. This thesis work provides a study of the effect that the realistic nuclear charge distributions may have on the frequency isotope shifts, as well as an estimate of whether this effect can be observed or not.

Since the realistic nuclear distributions were of major interest, it was necessary to initially obtain the most appropriate nuclear interaction predicting the finer details of the charge distributions. The so-called UDF1 set of Skyrme-parameters reproduces quite reliably the experimental results, displaying, for the rms radii and the most significant moment r^4, a mean value for the errors of the studied isotopes of the order of 1% and 6%, respectively. The corresponding errors for the higher order moments r^6 and r^8 were estimated to be 11% and 23%. A satisfactory enough theoretical representation of the higher order moments was important at this stage, since the isotope field shifts are approximated by an expansion

involving the first four even radial moments of the nuclear charge distributions.

Furthermore, we deduced that even if the parameters of the Fermi model can be tuned so that it reproduces realistic r^2 moments, this approximation does not accurately predict the higher r^4 and especially the r^6 and r^8 moments. The higher the order of the moment is, the more the Fermi model fails to approximate the moment of choice with high accuracy. For r^4 the error becomes 1% larger, whilst for r^6 and r^8 the error appears to be of a magnitude 5% and 15% larger, respectively. In order to estimate the field shifts $\delta\nu$, it is however the differences $\delta\left\langle r^{2N}\right\rangle$ between the radial moments of the isotopes that are needed. For these differences the errors may combine leading to overall increased uncertainty.

Separate field shift calculations were carried out for Fermi modeled and realistic higher moments, and the magnitude of the corrections $\delta\nu_{realistic} - \delta\nu_{Fermi}$ was examined for lithium like systems with spherical and deformed nuclei. In spherical nuclear systems, the magnitude of the corrections depends on the mass number. For the studied systems we found that the corrections can be considered as negligible when $A \lesssim 150$. On the contrary, in heavier systems the effect of the more realistic nuclear charge distributions becomes considerable and depends on the difference ΔN between the neutron numbers of the isotopes. In the heavy system of lead, that was of main interest in this thesis, the corrections add a contribution that reaches 0.26% for large ΔN. The corrections may become even more significant in lighter systems when the nuclei are deformed. A substantial increase of $\delta\nu_{realistic} - \delta\nu_{Fermi}$ was observed for Nd isotopes as deformation became larger. In the system of neodymium, when the target isotope is highly deformed, the contribution of the corrections to the field shift exceeds 1%. The corrections are due to density wiggles and variations in diffuseness that the Fermi model does not take into account, as well as -in the case of Nd isotopes- the deformed shape of the nucleus. These corrections can be important, depending on the required precision in the calculations of the field shift.

By comparing with observations in heavy systems, it is possible to extract the higher order radial moments of the nuclear charge distributions. The extraction of all four radial moments, which are taken into account in the expression of the reformulated field shift (RFS), requires four independent atomic transitions to be available. However, the sum of the expansion terms that gives the RFS can be re-arranged. A re-arrangement of the sum using an orthonormal basis finally leads to faster convergence. Eventually, the RFS is expressed as: $\delta\nu_{k,FS} = c_{k,1}\delta\left\langle y_1\right\rangle + c_{k,2}\delta\left\langle y_2\right\rangle$, where y_1 and y_2 depend on the first two moments r^2 and r^4. For two available transitions, the $\delta\left\langle r^2\right\rangle$ and $\delta\left\langle r^4\right\rangle$ can then be extracted.

In order to test the new method, theoretical field shifts were obtained by first calculating the nuclear densities and then solving for the electron orbitals. Using the calculated field shifts $\delta\nu_{FS}$ as pseudo-experimental-data, an attempt was made to invert the equations in order to extract the radial moments that contribute the most. It turns out that the extracted $\delta\left\langle r^2\right\rangle$ are almost identical to the corresponding theoretical values obtained from the nuclear HFB calculations. The displayed difference between the extracted $\delta\left\langle r^2\right\rangle$ and the $\delta\left\langle r^2\right\rangle_{HFB}$ is of the order of ~ 0.001 fm^2. Accordingly, the extracted $\delta\left\langle r^4\right\rangle$ are also in very good agreement with the $\delta\left\langle r^4\right\rangle_{HFB}$ values. However, the matrix equation that is solved is quite sensitive to the $\delta\nu_{FS}$ values. Therefore, the extracted $\delta\left\langle r^2\right\rangle$ and $\delta\left\langle r^4\right\rangle$ are to a great extent affected by the uncertainties in the observed isotope shifts (IS). In order to accurately obtain the $\delta\left\langle r^2\right\rangle$ and $\delta\left\langle r^4\right\rangle$, five correct digits are needed in the measurement of the IS for the ^{142,150}Nd isotope pair. Alternatively, a larger number of transitions must be available.

7 Outlook

In lithium like systems that were studied in this work only two, not entirely independent, transitions (same final state) are available experimentally. Moreover, in such systems the precision of the current experiments allows only three correct digits in the measurement of the IS. On the other hand, in neutral systems a larger number of independent transitions is normally accessible and thus, the extraction of $\delta\langle r^2\rangle$ and $\delta\langle r^4\rangle$ could be performed with higher precision. In addition, $\delta\langle r^6\rangle$ and $\delta\langle r^8\rangle$ could be possibly extracted by solving a system of four equations. Also, in neutral systems, the IS are in general measured with higher precision (four correct digits). The enhancement of the current experimental methods for the measurement of the IS will further facilitate the determination of the higher order nuclear moments. All in all, the re-arrangement of the summation that gives the RFS yields a novel method that allows the determination of the first two even nuclear radial moments, provided precise IS measurements. This method is also suitable in case more than two transitions are available, making it possible to extract even higher order moments so that we can subsequently draw further conclusions on the realistic properties of the nuclear charge distributions.

Acknowledgments I would like to thank my supervisors Gillis Carlsson and Jörgen Ekman for giving me the chance to work on this very interesting topic. I am happy and grateful to have worked with them. They were supportive and always ready to ably answer to any questions I had. Throughout this project, Gillis and Jörgen helped me to acquire valuable experiences and knowledge. I thank my family for providing me with all the help and support needed in order to be able to stay focus on my studies. Last but not least, I would like to thank my friends for their patience and support.

Self-reflection During the past six months that I have been working on this thesis I acquired knowledge in two fundamental fields of the physics science, nuclear and atomic physics. I learnt how crucial the development in one field of physics can prove to be for the progress in another field. Moreover, I realized how powerful the collaboration of theoretical and experimental studies is. I consider the knowledge and experiences valuable for my personal evolution and my professional career. I became more confident on how to work on a theoretical scientific problem and handle a long-term project. Further on, I gained experience in computer programming by utilizing the potential of computer power when performing theoretical calculations. All in all, this thesis work has equipped me with the necessary knowledge and theoretical background to pursue the career I always wanted in the current cutting-edge sectors of theoretical physics.

References

[1] I. Angeli. A consistent set of nuclear rms charge radii: properties of the radius surface r(n,z). *Atomic Data and Nuclear Data Tables*, 87(2):185 – 206, 2004.

[2] I. Angeli and K.P. Marinova. Table of experimental nuclear ground state charge radii: An update. *Atomic Data and Nuclear Data Tables*, 99(1):69–95, 2013.

[3] F. Aryasetiawan. Course litterature:"electronic structure theory". pages 24–25, 2014.

[4] B.G.Carlsson. Course litterature: "nuclear structure theory".

[5] S A Blundell, P E G Baird, C W P Palmer, D N Stacey, and G K Woodgate. A reformulation of the theory of field isotope shift in atoms. *Journal of Physics B: Atomic and Molecular Physics*, 20(15):3663, 1987.

[6] A. Bouyssy, J.-F. Mathiot, Nguyen Van Giai, and S. Marcos. Relativistic description of nuclear systems in the hartree-fock approximation. *Phys. Rev. C*, 36:380–401, 1987.

[7] B.G. Carlsson, J. Dobaczewski, J. Toivanen, and P. Veselý. Solution of self-consistent equations for the {N3LO} nuclear energy density functional in spherical symmetry. the program hosphe (v1.02). *Computer Physics Communications*, 181(9):1641–1657, 2010.

[8] P.Jönsson C.Froese Fischer, T.Brage. Computational atomic structure, an mchf approach, iop publishing, london uk (2000). page 12.

[9] Brandau et al. Isotope shift in the dielectronic recombination of three-electron $^{A}Nd^{57+}$. *Phys. Rev. Lett.*, 100(4):073201, 2008.

[10] J. Ekman et al. *To be published in Computer Physics Communications.*

[11] P. Jönsson, G. Gaigalas, J. Bieroń, C. Froese Fischer, and I.P. Grant. New version: Grasp2k relativistic atomic structure package. *Computer Physics Communications*, 184(9):2197–2203, 2013.

[12] C. Nazé, E. Gaidamauskas, G. Gaigalas, M. Godefroid, and P. Jönsson. ris3: A program for relativistic isotope shift calculations. *Computer Physics Communications*, 184(9):2187 – 2196, 2013.

[13] S.G. Nilsson and I. Ragnarsson. Shapes and shells in nuclear structure,cambridge university press, cambridge (1995). page 300.

[14] C W P Palmer. Reformulation of the theory of the mass shift. *Journal of Physics B: Atomic and Molecular Physics*, 20(22):5987, 1987.

[15] Randolf Pohl, Ronald Gilman, Gerald A. Miller, and Krzysztof Pachucki. Muonic hydrogen and the proton radius puzzle. *Annual Review of Nuclear and Particle Science*, 63(1):175–204, 2013.

[16] P. Ring and P. Schuck. The nuclear many-body problem, 1st ed. springer-verlag, new york, (1980). pages 217–218.

[17] P. Ring and P. Schuck. The nuclear many-body problem, 1st ed. springer-verlag, new york, (1980). pages 150–153.

[18] P. Ring and P. Schuck. The nuclear many-body problem, 1st ed. springer-verlag, new york, (1980). pages 175–176.

[19] R. Rosenfelder. Coulomb corrections to elastic electron–proton scattering and the proton charge radius. *Physics Letters B*, 479(4):381 – 386, 2000.

[20] E. C. Seltzer. k x-ray isotope shifts. *Phys. Rev.*, 188:1916–1919, 1969.

[21] V M Shabaev and A N Artemyev. Relativistic nuclear recoil corrections to the energy levels of multicharged ions. *Journal of Physics B: Atomic, Molecular and Optical Physics*, 27(7):1307, 1994.

[22] M.V. Stoitsov, N. Schunck, M. Kortelainen, N. Michel, H. Nam, et al. Axially deformed solution of the skyrme-h-f-b equations using the transformed harmonic oscillator basis (ii) hfbtho v2.00c:a new version of the program. *Comput.Phys.Commun.*, 184:1592–1604, 2013.

[23] J. Suhonen. From nucleons to nucleus, springer-verlag, berlin heidelberg (2007). pages 63–86.

[24] Shabaev V.M. Mass corrections in a strong nuclear field. *Theoretical and Mathematical Physics*, 63(3):588–596, 1985.

[25] H. De Vries, C.W. De Jager, and C. De Vries. Nuclear charge-density-distribution parameters from elastic electron scattering. *Atomic Data and Nuclear Data Tables*, 36(3):495 – 536, 1987.